Article

Cell

Induction of Autonomous Memory Alveolar Macrophages Requires T Cell Help and Is Critical to Trained Immunity

Graphical Abstract

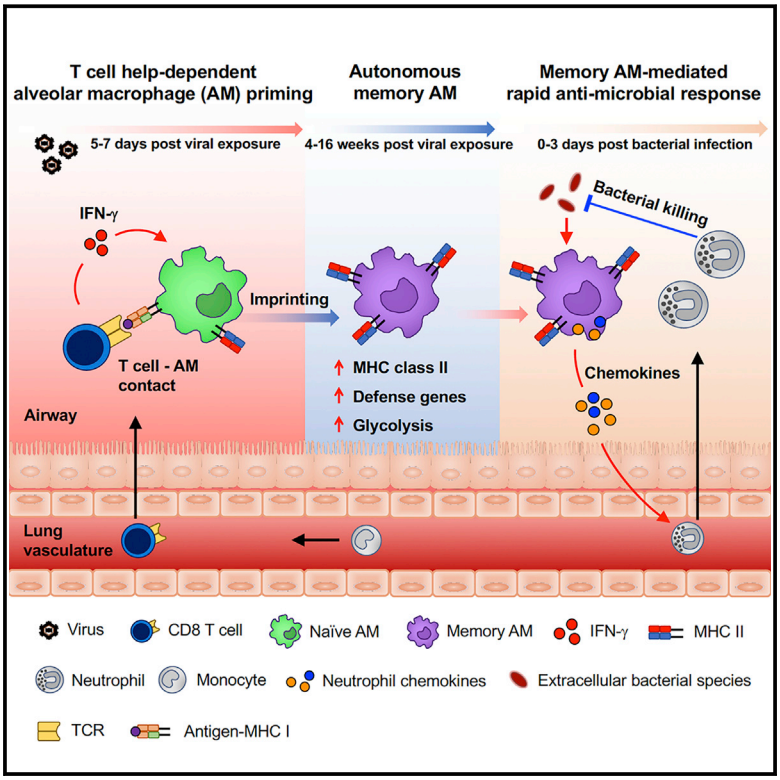

Highlights

- Respiratory viral infection induces lasting innate memory alveolar macrophages
- Memory alveolar macrophages develop and sustain independently of blood monocytes
- Adaptive T cells render innate macrophage memory via IFN-γ production
- Memory macrophages mediate trained anti-bacterial immunity via enhanced neutrophilia

Authors

Yushi Yao, Mangalakumari Jeyanathan, Siamak Haddadi, ..., Clinton S. Robbins, Jonathan D. Schertzer, Zhou Xing

Correspondence

xingz@mcmaster.ca

In Brief

The induction of self-renewing memory alveolar macrophages by viral infection requires priming by CD8 T cells, illustrating how signaling from adaptive to innate immune systems generates trained immunity key to protection from re-infection.

Yao et al., 2018, Cell *175*, 1634–1650
November 29, 2018
https://doi.org/10.1016/j.cell.2018.09.042

CellPress

Cell

Article

Induction of Autonomous Memory Alveolar Macrophages Requires T Cell Help and Is Critical to Trained Immunity

Yushi Yao,[1] Mangalakumari Jeyanathan,[1] Siamak Haddadi,[1] Nicole G. Barra,[2] Maryam Vaseghi-Shanjani,[1] Daniela Damjanovic,[1] Rocky Lai,[1] Sam Afkhami,[1] Yonghong Chen,[3] Anna Dvorkin-Gheva,[1] Clinton S. Robbins,[3] Jonathan D. Schertzer,[2] and Zhou Xing[1,4,*]

[1]McMaster Immunology Research Centre, M. G. DeGroote Institute for Infectious Disease Research, & Department of Pathology & Molecular Medicine, McMaster University, Hamilton, ON, L8S 4K1, Canada

[2]Department of Biochemistry and Biomedical Sciences & Farncombe Family Digestive Health Research Institute, McMaster University, Hamilton, ON, L8N 3Z5, Canada

[3]Peter Munk Cardiac Centre, Toronto General Research Institute, University Health Network, Toronto, ON, M5G 1L7, Canada

[4]Lead Contact

*Correspondence: xingz@mcmaster.ca

https://doi.org/10.1016/j.cell.2018.09.042

SUMMARY

Innate immune memory is an emerging area of research. However, innate immune memory at major mucosal sites remains poorly understood. Here, we show that respiratory viral infection induces long-lasting memory alveolar macrophages (AMs). Memory AMs are programed to express high MHC II, a defense-ready gene signature, and increased glycolytic metabolism, and produce, upon re-stimulation, neutrophil chemokines. Using a multitude of approaches, we reveal that the priming, but not maintenance, of memory AMs requires the help from effector CD8 T cells. T cells jump-start this process via IFN-γ production. We further find that formation and maintenance of memory AMs are independent of monocytes or bone marrow progenitors. Finally, we demonstrate that memory AMs are poised for robust trained immunity against bacterial infection in the lung via rapid induction of chemokines and neutrophilia. Our study thus establishes a new paradigm of immunological memory formation whereby adaptive T-lymphocytes render innate memory of mucosal-associated macrophages.

INTRODUCTION

Immunological memory represents a cardinal feature of the immune system (Farber et al., 2016) and has long been ascribed only to adaptive T and B lymphocytes in vertebrates (Farber et al., 2016). The instruction from innate antigen-presenting dendritic cells and macrophages is required for the initial priming and subsequent development of adaptive memory T cells (Guilliams et al., 2013a). Recent research, however, has challenged this dogma, revealing that following primary immunologic exposure, innate monocytes, macrophages, and NK cells may also be programed to carry an immune memory known as trained immunity when it enhances host defense (Cheng et al., 2014; Gourbal et al., 2018; Mitroulis et al., 2018; Netea et al., 2016). Such innate immune memory plays an important role in immunity against subsequent related or unrelated microbial exposure. However, our knowledge in innate immune memory at mucosal sites is scarce, and little is known about whether immune memory occurs in long-lived mucosal macrophages (Chen et al., 2014; Gourbal et al., 2018; Hamon and Quintin, 2016). In particular, the cellular mechanisms that locally initiate and instruct innate immune memory formation are still largely unclear.

The respiratory mucosa is frequently exposed to a broad range of pathogens, including adenoviruses, influenza, and *Streptococcus pneumoniae* (Eddens and Kolls, 2012; Kohlmeier and Woodland, 2009). To safeguard, it requires a robust innate immune system, including the mucosal surface alveolar macrophages (AMs) (Guilliams et al., 2013a; Hussell and Bell, 2014). Due to their unique location, AMs differ from other macrophage populations (Hussell and Bell, 2014). AMs turn over slowly and are of embryonic origin and self-maintained in steady state (Gomez Perdiguero et al., 2015; Guilliams et al., 2013b; Hoeffel et al., 2015). They are either replenished by or self-maintained during inflammation independently of circulating monocytes (Hashimoto et al., 2013; Machiels et al., 2017). While evidence shows that AMs imprinted by certain viral exposure such as influenza may lead to innate immune tolerance (Didierlaurent et al., 2008; Hussell and Bell, 2014; Machiels et al., 2017), it remains unclear whether and how AMs may be primed to carry an innate memory and act as an enhancer in anti-microbial host defense. New knowledge in this regard will shed light on innate immune memory in the mucosal immune system and foster effective mucosal immunization strategies (Jeyanathan et al., 2018; Low et al., 2015).

Here, by using murine models of acute respiratory viral infection, we investigated mucosal innate immune memory. We find that respiratory adenoviral infection induces long-term memory AMs characterized by high MHC II expression, a defense-ready gene signature, increased glycolytic metabolism, and heightened

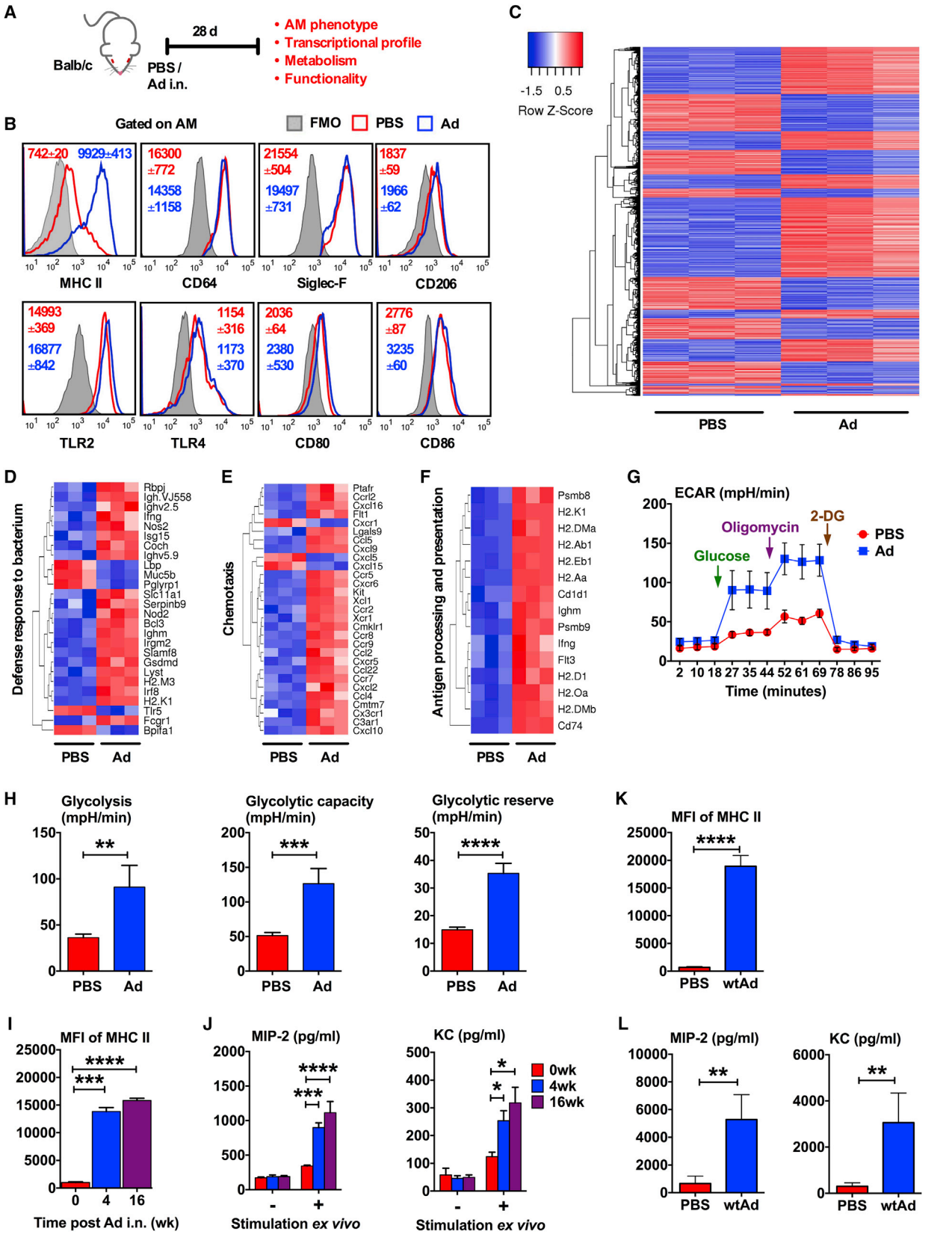

(legend on next page)

chemokine production. The priming, but not the maintenance, of memory AMs requires the help of effector CD8 T cells in an IFN-γ- and contact-dependent manner. The generation and maintenance of memory AMs are autonomous and involve a low rate of *in situ* proliferation independently of circulating monocytes or bone marrow progenitors. Finally, we find memory AMs to be critical to trained immunity against bacterial pathogens via rapid chemokine and neutrophilic responses. These findings establish a new paradigm of immunological memory formation, indicating that immunological memory may also develop in a reversed order of classical immunological memory formation (innate-to-adaptive memory), i.e., activated T cells can license innate immune memory of mucosal macrophages (adaptive-to-innate memory). Our study also shows a unique autonomous character of mucosal innate immune memory distinct from systemically acquired innate memory.

RESULTS

Acute Respiratory Viral Exposure Induces Alveolar Macrophages of Long-Lasting Memory Phenotype

The lung is equipped with mucosal surface AMs. To determine the impact of acute respiratory viral infection on AMs, BALB/c mice were infected intranasally (i.n.) with an adenoviral vaccine vector (Ad) (Smaill et al., 2013; Yao et al., 2017). At 4 weeks post-infection, airway AMs isolated by bronchoalveolar lavage were analyzed (Figure 1A). A comprehensive gating strategy (Hussell and Bell, 2014; Misharin et al., 2013) was used to distinguish bona fide AMs (Ly6G$^-$CD11b$^-$CD11c^{hi}CD64^{hi}Siglec-F^{hi}) from other myeloid cells, including dendritic cells (DCs), monocyte-derived macrophages (MDMs), and interstitial macrophages (IMs) in the lung (Figure S1A). Compared to naive AMs, AMs from viral-infected lung expressed high levels of MHC II (MHC II^{hi} AM) (Figure 1B). Other AM surface markers Siglec-F, CD64, and CD206, activation markers TLR2/4 and CD80/86 (Figure 1B), and CD11b and CD11c (Figure S1B) remained unchanged. Using RNA-based gene microarray, AMs from infected lungs were shown to exhibit marked differences from naive AMs in transcriptional profiles (Figure 1C). Notably, the majority of the genes related to host defense (defense responses, chemotaxis, and antigen presentation) were markedly upregulated in MHC II^{hi} AMs (Figures 1D–1F and Tables S1, S2, and S3). Such AMs also demonstrated markedly increased glycolytic metabolism (Figures 1G and 1H).

We next addressed whether virus-induced MHC II^{hi} AMs were long-lasting. AM MHC II^{hi} phenotype persisted to 4 and 16 weeks post-infection (Figure 1I). Given the transient nature of respiratory adenoviral infection (Xing et al., 2000), these data indicate the emergence of a persisting memory phenotype of AM poised for enhanced host defense. To study this further, AMs were isolated from naive and 4- and 16-week viral-infected lungs and cultured *ex vivo* with or without stimulation by live *S. pneumoniae*. Compared to unstimulated naive AMs, unstimulated 4- and 16-week memory AMs did not release increased neutrophil chemokines MIP-2 and KC. In contrast, bacterium-stimulated 4- and 16-week memory AMs produced significantly more MIP-2 and KC than their stimulated naive counterparts (Figure 1J).

We further examined whether memory AMs would develop following respiratory infection by wild-type adenovirus (wtAd). At 4 weeks post-infection, abundant MHC II^{hi} AMs were detected in wtAd-infected lungs (Figure 1K), and they readily released MIP-2 and KC upon *ex vivo* bacterial stimulation (Figure 1L). The above data show that viral exposure elicits long-lasting memory AMs characterized by high MHC II expression, a defense-ready gene signature, increased glycolytic metabolism, and heightened neutrophil chemokine responses.

Memory AMs Develop and Self-Sustain Independently of Circulating Monocytes

AMs are of embryonic origin and self-sustained in steady state but are maintained with the contribution from blood monocytes during inflammation (Guilliams et al., 2013b; Machiels et al., 2017). However, evidence also suggests AMs to be maintained independently of monocytes under inflammatory conditions (Hashimoto et al., 2013). We next examined the kinetics of memory AM development and its relationship to circulating monocytes. At various time points post-viral infection (Figure 2A), compared to naive animals (day 0), numbers of total AMs in the airway (BAL) and lung tissue remained constant except at days 7 and 14 when they temporarily declined (Figure 2B), which coincided with mildly increased AM apoptosis (Figure 2C). By day 28, numbers of AMs returned to levels in naive animals (Figure 2B). However, AMs did not acquire MHC II^{hi} phenotype until day 7, which remained constant between days 7 and 28 (Figure 2D) and

Figure 1. Acute Respiratory Viral Exposure Induces AM of Long-Lasting Memory Phenotype

(A) Schema of respiratory viral infection. Mice were treated intranasally (i.n.) with adenoviral vaccine vector (Ad), wild-type adenovirus (wtAd), or PBS.

(B) Histograms of expression of MHC II and other AM activation surface markers at 4 weeks post-infection. Numbers in histograms are mean ± SD of median fluorescence intensity (MFI).

(C) Hierarchical clustering and heatmap of 2,408 out of 31,873 RNA transcripts differentially expressed in AM of 4-week PBS and viral-infected mice.

(D–F) Heatmaps of genes related to host defense (D), chemotaxis (E), and antigen presentation (F) in AM of 4-wk PBS and viral-infected mice.

(G) Real-time extracellular acidification rate (ECAR) in AM at 4 weeks post-infection. 2-DG: 2-deoxy-glucose.

(H) Glycolysis, glycolytic capacity and glycolytic reserve in AM at 4 weeks post-infection.

(I) MFI of MHC II expression on AM at 0, 4 and 16 weeks post-infection.

(J) MIP-2 and KC contents in supernatants of cultured AM with or without *S. pneumoniae* at 0, 4, 16 weeks post-infection.

(K) MFI of MHC II expression on AM at 4 weeks post-wtAd infection.

(L) MIP-2 and KC contents in supernatants of *S. pneumoniae*-stimulated AM at 4 weeks post-wtAd infection.

Data in (B) and (I)–(L) are representative of two independent experiments (n = 3 mice/group). Data in (C) –(F) are from one experiment (n = 3 mice/group). Data in (G) and (H) are representative of three independent experiments (n = 4 wells/group). Bar graphs and data in (G) are presented as mean ± SD. *$p < 0.05$; **$p < 0.01$; ***$p < 0.001$; ****$p < 0.0001$.

See also Figure S1 and Tables S1, S2, and S3.

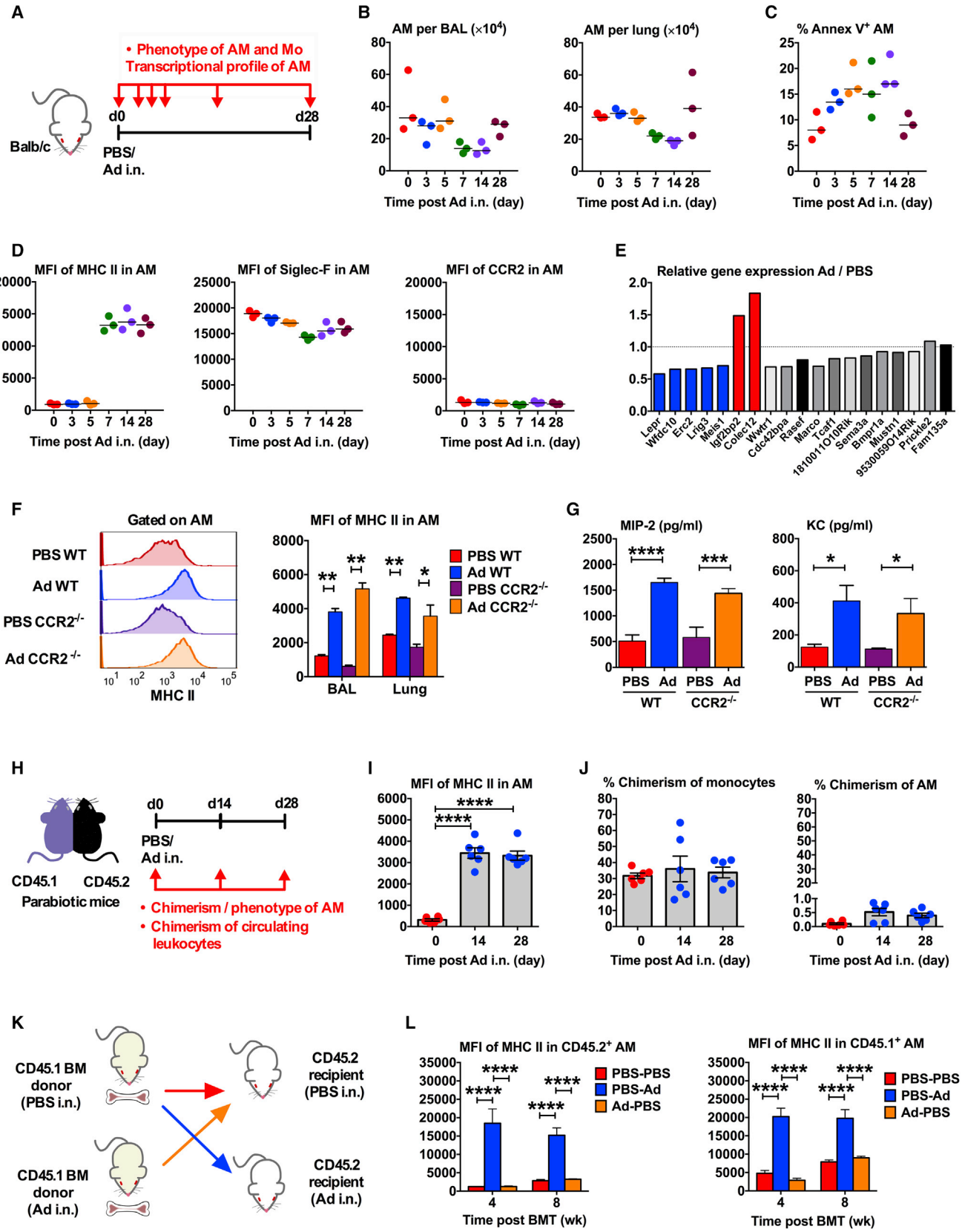

(legend on next page)

persisted up to 16 weeks (Figure 1I). We next analyzed the kinetic expression of Siglec-F and CCR2 in AMs post-infection to examine whether MHC II^{hi} AMs were of lung residential (embryonic, Siglec-F^{hi}) or monocytic (CCR2^{hi}) origin (Machiels et al., 2017). Siglec-F on MHC II^{hi} AMs from day 7 onward was as comparably high as MHC II^{low} AMs of earlier time points (Figure 2D). On the other hand, CCR2 expression on AMs was minimal throughout between days 0 and 28 (Figure 2D) irrespective of MHC II levels. These data suggest a lung residential, as opposed to monocytic, origin of memory AMs. To support further, we compared the profiles of embryonic signature genes (Machiels et al., 2017) in naive versus day 28 memory AMs. Memory AMs expressed the majority of embryonic genes (12/19) similar to expression levels in naive AMs of embryonic origin (Figure 2E, gray/black bars), with only 5/19 being significantly lower than in naive AMs (Figure 2E, blue bars), different from monocyte-derived AMs that do not significantly express most of these genes (16/20) (Machiels et al., 2017). Furthermore, circulating monocytes of infected and naive mice did not differ in expression of MHC II, CD206, TLR2/4, and CD80/86 (Figure S2A). Our data thus far argue against a monocytic origin of memory AMs.

To further study the independence of memory AMs on circulating monocytes, we used CCR2$^{-/-}$ mice lacking classical Ly6-C^{hi} monocytes, a major contributor to tissue monocyte-derived macrophages (Epelman et al., 2014). In the absence of such monocytes (Figure S2B), compared to 4-week infected WT mice (Ad WT), infected CCR2$^{-/-}$ mice (Ad CCR2$^{-/-}$) had an unimpaired ability to develop and maintain MHC II^{hi} AM in the airway (BAL) and lung (Figure 2F), consistent with uncompromised total AM (Figure S2C). Upon bacterial stimulation, memory AMs of infected CCR2$^{-/-}$ mice produced comparably heightened chemokines (Figure 2G). To exclude the potential contribution of Ly6C^{low} monocytes to memory AMs (Sabatel et al., 2017), we depleted Ly6C^{low} monocytes in CCR2$^{-/-}$ mice by i.v. deliveries of clodronate liposomes (CL) post-infection (Figure S2D). Generation of memory AMs at day 7 post-infection remained intact in the absence of both Ly6C^{hi} and Ly6C^{low} monocytes (Figure S2E), as shown by unaltered levels of MHC II, chemokines, and AMs compared to infected WT controls (Figures S2F–S2H).

Using a parabiosis approach with CD45.1 and CD45.2 congenic mice (Figure 2H), the conjoined mice were shown to develop MHC II^{hi} AMs in the respective airway at days 14 and 28 post-viral exposure (Figures 2I and S2I). Of importance, while via the shared blood flow, parabionts developed expected high levels of chimerism in circulating monocytes (on average 30%–40%) (Figures 2J and S2J) and other circulating immune cells (Figure S2K) before and after viral infection, there was consistently minimal chimerism (on average ≈0.5%) in AMs in the respective airway of parabionts at days 14 and 28 (Figures 2J and S2J). In other words, only about 1%–2% of memory AMs were monocyte-derived. The above data indicate that circulating monocytes contribute minimally to memory AM generation or maintenance.

Recent studies suggest that systemic immune activation may imprint myeloid progenitors in bone marrow (BM), which could give rise to trained monocytes or even macrophages (Kaufmann et al., 2018; Mitroulis et al., 2018). To further demonstrate the independence of memory AM development on both blood monocytes and BM myeloid progenitors, we employed a BM chimeric approach. By this approach, irradiation ablates all BM progenitor cells and blood monocytes in recipient mice while it still spares some recipient's AMs due to their radio-resistance (Hashimoto et al., 2013; Hussell and Bell, 2014), thus allowing examination of whether established recipient's memory AMs could self-sustain in the absence of both BM progenitors and blood monocytes. Thus, the 3-way CD45.1 and CD45.2 congenic BM chimeric mice (Figure 2K) were produced: CD45.1 PBS donor BM engrafted into CD45.2 PBS recipients (PBS-PBS) as control; CD45.1 PBS donor BM into CD45.2 Ad recipients (PBS-Ad); and CD45.1 Ad donor BM into CD45.2 PBS recipients (Ad-PBS). Indeed, while irradiation eliminated all recipient's own monocytes and neutrophils with most of them being donor-derived (CD45.1+) (Figure S3A), 10%–25% of total AMs in 3 types of BM chimeras remained to be of recipient origin (CD45.2+), and their numbers remained comparable over 4–8 weeks post-BM transplantation (BMT) (Figures S3B and S3C). Of importance, only the lung of viral-infected recipients (PBS-Ad) harbored sustained recipient-derived MHC II^{hi} AMs (CD45.2^{+}) over 4 and 8 weeks post-BMT (Figure 2L) despite lacking recipient-derived

Figure 2. Memory AM Develop and Self-Sustain Independently of Circulating Monocytes

(A) Schema of kinetic analysis in AM and monocytes (Mo) post-viral infection.

(B) Numbers of total AM in BAL and lung at various time points post-infection.

(C) Frequencies of Annex V^{+} AM at various time points post-infection.

(D) MFI of MHC II, Siglec-F and CCR2 expression on AM at various time points post-infection.

(E) Relative expression of embryonic-derived signature genes in AM from viral-infected lungs over that from PBS controls. Shaded gray and black bars indicate the genes not differentially expressed between the two groups. Red and blue bars are significantly up-and downregulated genes, respectively.

(F) Representative histograms and MFI of MHC II expression on AM from WT and CCR2$^{-/-}$ mice at 4 weeks post-PBS or infection.

(G) MIP-2 and KC contents in supernatants of *S. pneumoniae*-stimulated AMs from 4-week WT and CCR2$^{-/-}$ mice.

(H) Schema of parabiotic mouse model of viral infection. Both congenic mice were infected.

(I) MFI of MHC II expression on AM in parabionts at days 0, 14 and 28 post-infection.

(J) Chimerism of blood monocytes and AM in parabionts at days 0, 14 and 28 post-infection.

(K) Schema of 3-way bone marrow (BM) chimeric mice.

(L) MFI of MHC II expression on AM of recipient (CD45.2^{+}) or donor (CD45.1^{+}) origin in BM chimera at 4 and 8 weeks post-BM transplantation (BMT).

Horizontal lines in (B)–(D) are median values. Bar graph in (E) shows average fold changes. Bar graphs in (F), (G), and (L) are presented as mean ± SD and in (I) and (J) as mean ± SEM. Data in (B)–(D), (F), (G), (I), and (J) are representative of two independent experiments (B–D, F, and G: n = 3 mice/group; I and J: n = 6 mice/group). Data in (E) and (L) are from one experiment (E: n = 3; L: n = 5 mice/group). *p < 0.05; **p < 0.01; ***p < 0.001; ****p < 0.0001.

See also Figures S2 and S3.

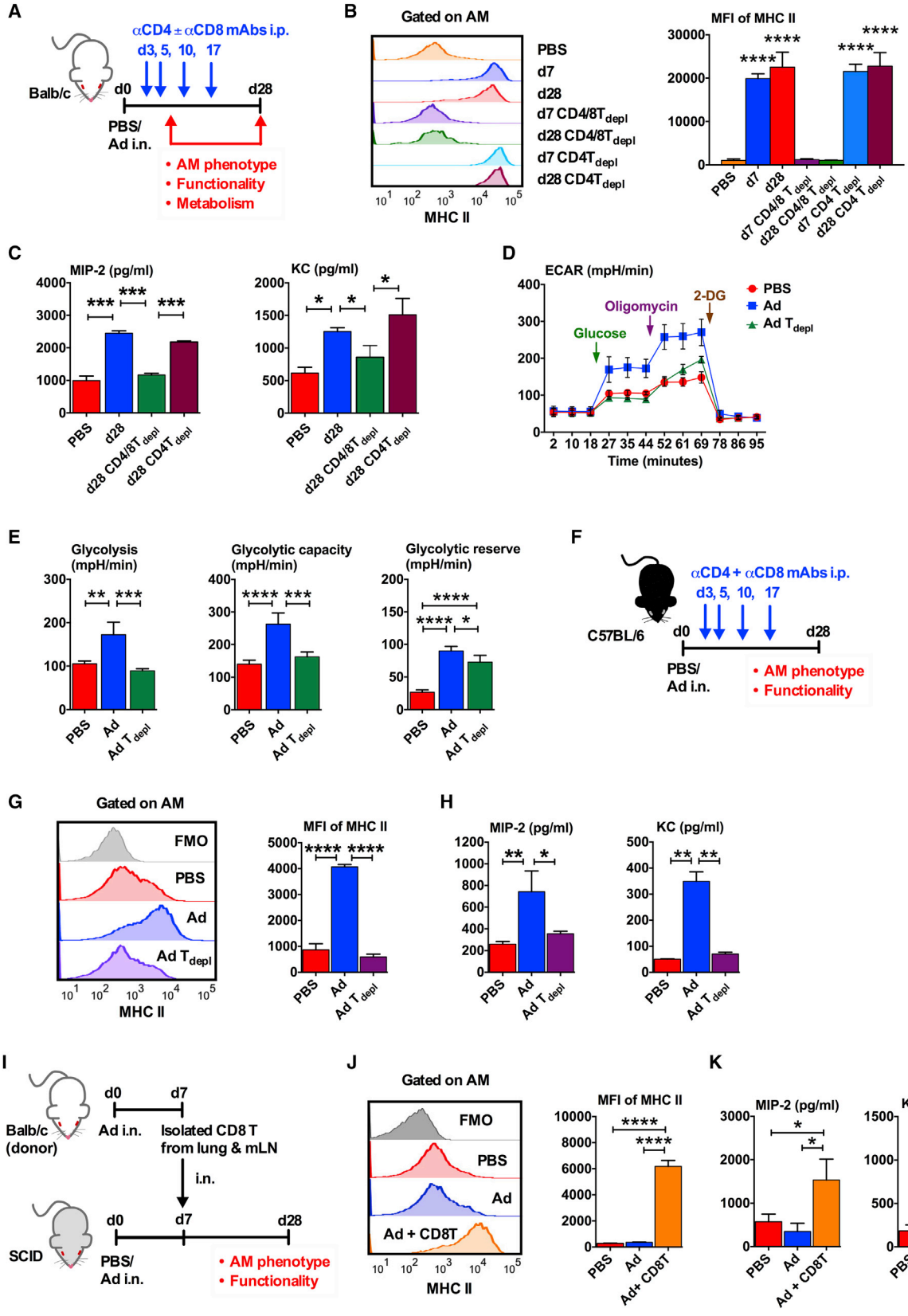

(legend on next page)

BM progenitors and monocytes (Figure S3A). Donor-derived MHC II^{hi} AM (CD45.1^{+}) were also found in PBS-Ad lungs (Figure 2L), likely due to irradiation-related artificial AM re-population (Hashimoto et al., 2013; Hussell and Bell, 2014). Like PBS-PBS control BM chimeras, Ad-PBS BM chimera had few MHC II^{hi} AMs of either recipient or donor origin post-BMT (Figure 2L).

Given the autonomous nature of memory AMs, we determined if *in situ* proliferation was a mechanism to maintain memory AMs. We found 10%–12% of AMs labeled with BrdU following airway BrdU delivery and 44%–49% of them being Ki-67^{+} in day 14- or 28-infected animals comparable to un-infected controls (Figure S3D). Together, the above data indicate that AMs assume a MHC II^{hi} phenotype between 5 and 7 days post-viral infection. Memory AMs are autonomous, and they develop and self-sustain locally, independently of circulating monocytes and/or BM progenitors.

CD8 T Cell Help Is Required for Priming, but Not Maintenance, of Memory AMs

Thus, airway MHC II^{hi} AMs began to develop between 5–7 days in the effector phase of anti-viral responses (Figure 2D), coincided with the entry of virus-induced T cells, in particular CD8 T cells, into the airway, which began at day 3 and rose markedly by day 7 (Figure S4A). To further investigate the mechanisms of memory AM generation, we determined whether T cells and which T cell subset were involved in the priming of memory AMs. Thus, CD4 T and/or CD8 T cells were depleted *in vivo* from day 3 onward post-infection, and their depletion was maintained via repeated injections of anti-CD4 and CD8 monoclonal antibodies (mAbs) to viral-infected BALB/c mice (Figures 3A, S4B, and S4C). Lack of both CD4 and CD8 T cells resulted in loss of memory AM at either day 7 or 28 (Figures 3B and 3C, day 7 CD4/8T$_{depl}$ or day 28 CD4/8T$_{depl}$). In contrast, depletion of CD4 T cells alone failed to do so (Figures 3B and 3C, day 7 CD4T$_{depl}$ or day 28 CD4T$_{depl}$). Alongside loss of MHC II and chemokine markers (Figures 3B and 3C) was loss of the metabolic signature in AMs of T-cell-depleted hosts as shown by markedly diminished glycolysis (Figure 3D and 3E).

We next determined if memory AMs could develop in a T-cell-dependent manner following respiratory viral infection in C57BL/6 mice genetically distinct from BALB/c mice (Figure 3F). As in BALB/c mice (Figures 3A–3C), MHC II^{hi} AM developed following viral infection in B6 mice (Ad), whereas CD4 and CD8 T cell depletion (Ad T$_{depl}$) abrogated its formation (Figure 3G) and chemokine production (Figure 3H).

To further investigate the requirement of CD8 T cells in priming of AM memory, SCID mice were viral-infected for 7 days, airway-transferred with CD8 T cells purified from day 7 viral-infected donor BALB/c mice, and analyzed at day 28 (Figure 3I). As the case of day 28 CD4 and CD8 T cell-depleted BALB/c mice (Figures 3B and 3C), infected SCID mice (Ad) failed to develop MHC II^{hi} AMs (Figure 3J), and their AMs failed to produce chemokines upon re-stimulation (Figure 3K). However, transferring CD8 T cells to the airway of infected SCID hosts (Ad+CD8T) restored memory AMs both phenotypically and functionally (Figures 3J and 3K).

Since the adenovirus used in this study elicits long-lasting memory CD8 T cells in the airway (Jeyanathan et al., 2010), we determined the role of T cells in the maintenance phase of memory AMs. Thus, following viral infection, memory AMs were allowed to develop in the airway of BALB/c mice, and CD4 and CD8 T cells were then depleted from day 28 onward by repeated anti-T cell mAb injections (Figures S4D–S4F). T cell depletion, after memory AMs were fully developed, had little impact on the maintenance of MHC II^{hi} AM (Figure S4G, Ad T$_{depl}$ day 28), nor did it hinder their numbers or chemokine production (Figures S4H and S4I, Ad T$_{depl}$ day 28). AMs were not affected by anti-CD4 mAb, as they expressed no CD4 (Figures S4I and S4J). The above data indicate that the help from viral-induced CD8 T cells is required for the priming, but not maintenance, of memory AMs. Memory AMs develop within a window during the effector phase of host responses.

CD8 T Cells Prime the Formation of Memory AMs via IFN-γ Production

As IFN-γ is an effector cytokine from CD8 T cells and a prototypic macrophage activator (Barton et al., 2007) and in our model, CD8 T cells produced abundant IFN-γ in the effector phase of anti-viral host responses (Figures S5A and S5B), we determined the role of IFN-γ in CD8 T cell-mediated priming of memory AMs. Thus, WT B6 (WT Ad) and IFN-$\gamma^{-/-}$ (IFN-$\gamma^{-/-}$ Ad) mice were viral-infected, and a group of IFN-$\gamma^{-/-}$ mice were also supplied i.n. with recombinant IFN-γ (IFN-$\gamma^{-/-}$ Ad+rIFN-γ) between days 4 and 10 post-infection (Figure 4A).

Figure 3. CD8 T Cell Help Is Required for Priming, but Not Maintenance, of Memory AMs

(A) Schema of CD4 T and CD8 T cell depletion by intraperitoneal (i.p.) injections of mAbs in effector phase of host responses to viral infection in BALB/c mice.
(B) Representative histograms and MFI of MHC II expression on AM at day 7 or 28 post-infection without or with depletion of CD4/CD8 T cells or only CD4 T cells.
(C) MIP-2 and KC contents in supernatants of *S. peumoniae*-stimulated AM from 4-week PBS or infected mice with or without T cell depletion.
(D) Real time extracellular acidification rate (ECAR) in AM at 4 weeks post-infection with or without depletion of CD4/CD8 T cells. 2-DG: 2-deoxy-glucose.
(E) Glycolysis, glycolytic capacity and glycolytic reserve in AM at 4 weeks post-infection with or without depletion of CD4/CD8 T cells.
(F) Schema of CD4/CD8 T cell depletion in effector phase of host responses to viral infection in C57BL/6 mice.
(G) Representative histograms and MFI of MHC II expression on AM of C57BL/6 mice at day 28 post-infection with or without depletion of CD4/CD8 T cells.
(H) MIP-2 and KC contents in supernatants of *S. pneumoniae*-stimulated AM from C57BL/6 mice with or without T cell depletion.
(I) Schema of adoptive transfer of CD8 T cells from day 7 infected donor BALB/c mice into the airway of day 7 infected SCID mice in effector phase of host responses.
(J) Representative histograms and MFI of MHC II expression on AM at day 28 post-infection in SCID mice with or without CD8 T cell transfer.
(K) MIP-2 and KC contents in supernatants of *S. pneumoniae*-stimulated AM from day 28 infected SCID mice with or without CD8 T cell transfer.
Bar graphs and data in (D) are presented as mean ± SD. Data are representative of two independent experiments (B, C, G, H, J, and K: n = 3 mice/group; D and E: n = 4 wells/group) *p < 0.05; **p < 0.01; ***p < 0.001; ****p < 0.0001.
See also Figure S4.

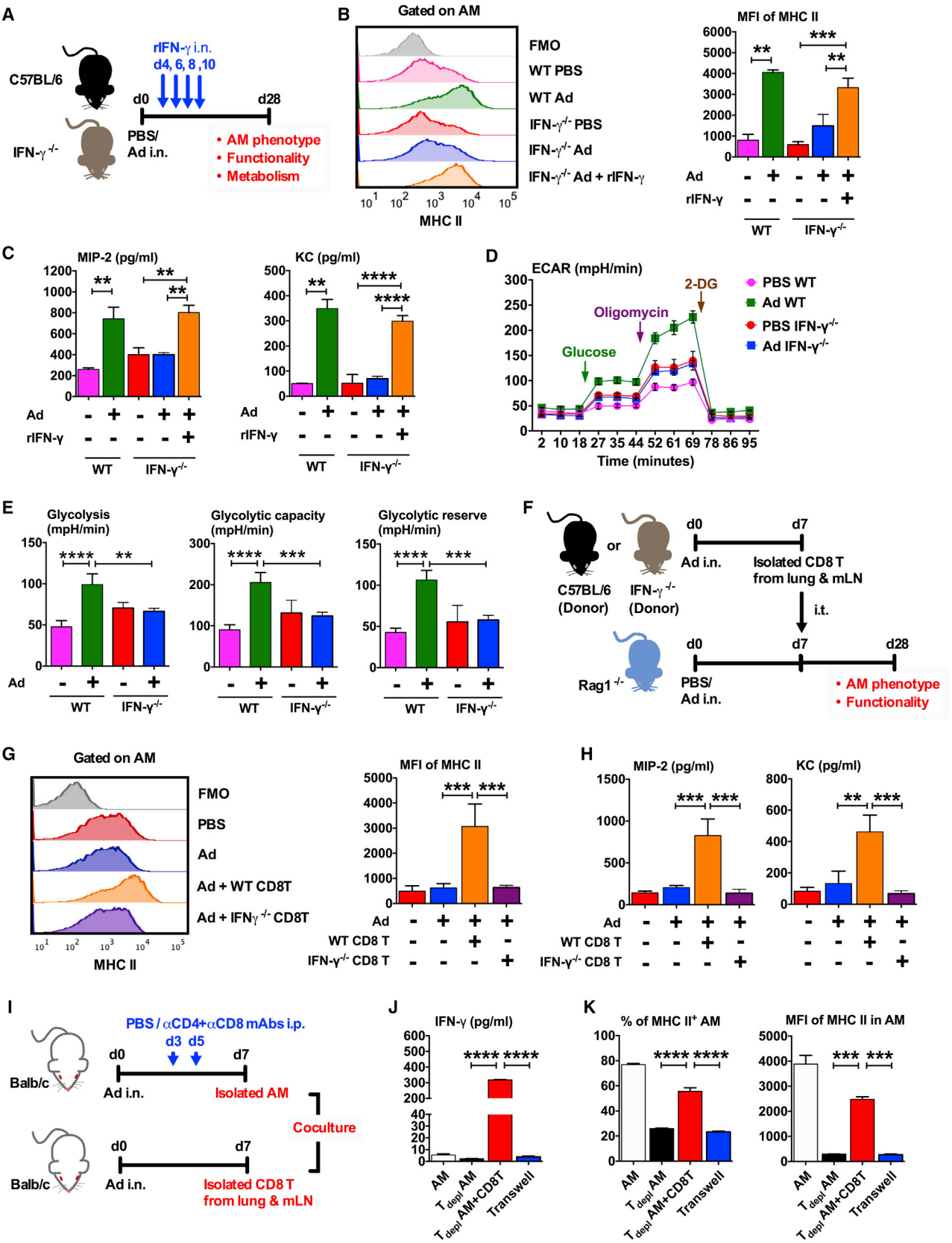

(legend on next page)

Compared with WT Ad mice, IFN-γ deficiency (IFN-$\gamma^{-/-}$ Ad) led to the loss of MHC II^{hi} AM (Figure 4B), blunted chemokine production (Figure 4C)m and diminished glycolytic metabolism (Figure 4D and 4E). However, IFN-γ reconstitution in the effector phase in infected IFN-$\gamma^{-/-}$ mice (IFN-$\gamma^{-/-}$Ad+rIFN-γ) rescued memory AM generation (Figure 4B and 4C). Likewise, IFN-γ receptor deficiency (IFN-γ$R^{-/-}$) led to impaired memory AM generation post-infection (Figures S5C–S5E). These data show a critical role of IFN-γ in the generation of memory AMs following viral infection.

We next determined whether it was CD8 T-cell-derived IFN-γ involved in AM priming. Effector CD8 T cells were purified from lungs and draining lymph nodes (mLN) of day 7 viral-infected WT and IFN-$\gamma^{-/-}$ mice and transferred intratracheally (i.t.) into the airway of day 7-infected Rag1$^{-/-}$ recipient mice (Figure 4F). Consistent with the data from SCID mouse model (Figures 3I–3K), as in uninfected Rag1$^{-/-}$ mice (PBS), T cell deficiency led to lack of memory AM in infected Rag1$^{-/-}$ mice (Ad) (Figures 4G and 4H, blue histogram/bars), whereas reconstitution with virus-activated WT effector CD8 T cells (Ad+WT CD8T) rescued memory AM formation (Figures 4G and 4H). In contrast, reconstitution with IFN-$\gamma^{-/-}$ effector CD8 T cells (Ad + IFN$\gamma^{-/-}$CD8T) failed to do so (Figures 4G and 4H). These data indicate that IFN-γ from effector CD8 T cells is critical to memory AM formation.

Given the juxtaposition of AMs and T cells on the surface of respiratory mucosa, we determined whether memory AM formation required T cell-AM contact using a transwell co-culture approach. This approach also helped address whether antigen presentation to T cells by activated AMs was likely involved in T cell IFN-γ production. Thus, two groups of BALB/c mice were viral-infected. One group was T cell-competent PBS control, and another was depleted of effector T cells via injection of mAbs at days 3 and 5 to block AM priming. Un-primed airway AMs isolated at day 7 were then co-cultured in contact with effector CD8 T cells isolated from day 7-infected mice (Figure 4I). Separately, the un-primed AMs were cultured with effector CD8 T cells but physically separated within transwells. After 24 hr culture, T cells released markedly increased IFN-γ only when in contact with AM (T_{depl} AM+CD8T) (Figure 4J). Similarly, a significant increase in MHC II^{hi} AMs was observed only when in direct contact with CD8 T cells (T_{depl} AM+CD8T) (Figure 4K). The transwell separation of the two abolished induction of MHC II^{hi} AMs (Transwell) (Figure 4K). The above data suggest that CD8 T cells prime for AM memory in the airway via IFN-γ production, and AM-T cell contact is required for this process.

Memory AMs Are Associated with Long-Lasting Trained Immunity against Bacterial Infection

We next sought to determine the physiological relevance of viral-induced innate immune memory in AMs. This is important, as it is known that influenza causes the immune tolerance of lung macrophages and impairs anti-bacterial host defense (Didierlaurent et al., 2008). Since one hallmark of innate immune memory is its ability, via re-programed innate immune cells, to enhance non-specific innate protection against heterologous microbial infection (Arts et al., 2018; Gourbal et al., 2018), we examined whether the memory AM-bearing lung was better protected from infection by *S. pneumoniae*, a common respiratory bacterial pathogen (Eddens and Kolls, 2012). Thus, at 4 weeks post-viral exposure, we challenged BALB/c mice i.t. with a lethal dose of *S. pneumoniae* (Figure 5A). A significantly improved survival was observed in viral-exposed mice (Ad) over PBS control (Figure 5B), associated with markedly improved clinical outcomes (illness scores and body weight losses) at 48 and 72 hr post-bacterial infection (Figure 5C). Furthermore, compared to PBS controls, bacterial colony forming units (CFU) in the lung were 1.5, 2, and 2.5 log lower at 24, 48, and 72 hr, respectively (Figure 5D). Much reduced CFU was also seen in the spleen (Figure 5D). While a pronounced cellular response was seen in the peri-bronchial regions of viral-exposed mice at 24 hr, much reduced lung histopathology, particularly at 72 hr, was readily discernible (Figure 5E). Thus, induction of memory AMs following viral exposure is associated with trained immunity against *S. pneumoniae* infection in the lung.

Since memory AMs are long-lasting (Figure 1I and 1J), we next determined the longevity of trained immunity. Viral-exposed BALB/c mice were challenged at 6, 8, and 16 weeks with a lethal dose of *S. pneumoniae*. Compared to PBS control, bacterial CFU of 6, 8, or 16 weeks viral-exposed mice were markedly reduced in the lung and spleen (Figure 5F) similar to that in 4-week viral-exposed animals (Figure 5D).

Figure 4. CD8 T Cells Prime the Formation of Memory AM via IFN-γ Production

(A) Schema of WT C57BL/6 and IFN-$\gamma^{-/-}$ mouse model of viral infection. Recombinant murine IFN-γ (rIFN-γ) was delivered i.n. to some IFN-$\gamma^{-/-}$ mice.

(B) Representative histograms and MFI of MHC II expression on AM at day 28 post-infection in WT and IFN-$\gamma^{-/-}$ mice with or without rIFN-γ.

(C) MIP-2 and KC contents in supernatants of *S. pneumoniae*-stimulated AM from day 28 infected WT or IFN-$\gamma^{-/-}$ mice with or without rIFN-γ.

(D) Real time extracellular acidification rate (ECAR) in AM at day 28 post-infection in WT or IFN-$\gamma^{-/-}$ mice. 2-DG: 2-deoxy-glucose.

(E) Glycolysis, glycolytic capacity and glycolytic reserve in AM at day 28 post-infection in WT or IFN-$\gamma^{-/-}$ mice.

(F) Schema of Rag-1$^{-/-}$ mouse model with or without donor WT or IFN-$\gamma^{-/-}$ CD8 T cells transferred i.t. to the airway in effector phase of host responses to viral infection.

(G) Representative histograms and MFI of MHC II expression on AM at day 28 post-infection in Rag1$^{-/-}$ mice with or without receiving donor WT or IFN-$\gamma^{-/-}$ CD8 T cells.

(H) MIP-2 and KC contents in supernatants of *S. pneumoniae*-stimulated AM from Rag1$^{-/-}$ mice with or without receiving donor WT or IFN-$\gamma^{-/-}$ CD8 T cells.

(I) Schema of AM and CD8 T cell co-culture with or without using transwell. AM were from day 7 infected BALB/c mice with or without earlier T cell depletion. CD8 T cells were from day 7 infected BALB/c mice.

(J) IFN-γ contents by T cells at 24 hr post-co-culture with AM in direct contact or separation in transwell.

(K) Frequencies of MHC II^{hi} AM and MFI of MHC II on AM at 24 hr post-*ex vivo* co-culture with or without CD8 T cells, and in direct contact or separation in transwell.

Bar graphs and data in (D) are presented as mean ± SD. Data are representative of two independent experiments (B, C, G, and H: n = 3 mice/group; D and E: n = 4 wells/group; J and K: 3 wells/group). **p < 0.01; ***p < 0.001; ****p < 0.0001.

See also Figure S5.

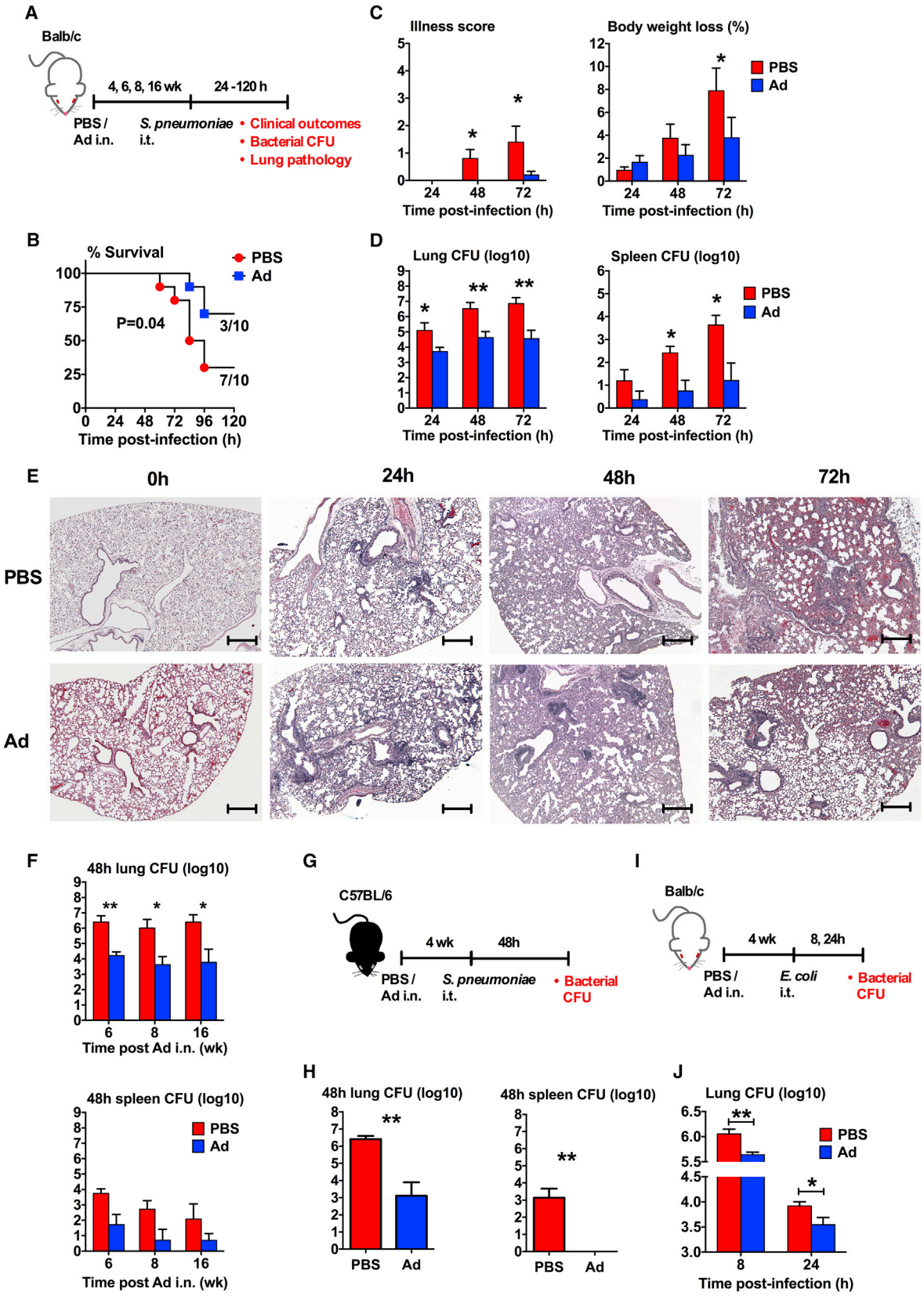

(legend on next page)

As memory AMs developed following viral exposure in either BALB/c or B6 mice (Figures 1, 2, 3, and 4), we also examined anti-bacterial trained immunity in 4-week viral-exposed C57BL/6 mice (Figure 5G). Levels of *S. pneumoniae* infection of B6 mice were much reduced in the lung and spleen at 48 hr post-infection (Figure 5H). To address whether trained immunity in the lung could help control infection by other bacterial species than *S. pneumoniae*, 4-week viral-exposed BALB/c mice were infected with Gram-negative *E. coli* (Figure 5I). Indeed, trained immunity also significantly reduced *E. coli* infection in the lung at 8 and 24 hr post-infection (Figure 5J).

Since effector T cell depletion in the priming phase of AMs impeded memory AM formation (Figures 3A–3E), this model offered an opportunity to study the causality between memory AMs and anti-bacterial trained immunity. Thus, BALB/c mice were viral-exposed, depleted of total T cells, and at day 28 were infected with *S. pneumoniae* (Figure S6A). In contrast to T cell competent control (Ad), lack of memory AMs due to T cell depletion in the priming phase (Ad T_{depl} day 3) led to loss of anti-bacterial trained immunity in the lung (Figure S6B).

Previous studies suggest the virus-induced memory T cells to directly and non-specifically enhance anti-microbial innate protection (Berg et al., 2003; Strutt et al., 2010). Since the adenovirus elicits memory CD8 T cells in the airway (Jeyanathan et al., 2010) and depletion of T cells after memory AMs had fully developed does not affect the maintenance of memory AM (Figure S4F–S4I), we sought to establish that anti-bacterial trained immunity could operate fully independently of virus-induced memory T cells. Thus, total T cells were depleted of day 27 viral-exposed mice and followed by challenge with *S. pneumoniae* (Figure S6C). Compared to PBS control, T cell-depleted mice (Ad T_{depl} day 27) were as well protected as memory T cell competent hosts (Ad) (Figure S6D). The above data suggest that memory AMs is associated with anti-bacterial trained immunity in the lung and virus-induced memory T cells do not directly contribute to this process.

Trained Immunity Augments Anti-bacterial Protection via Accelerated Chemokine Responses and Neutrophilia in the Lung

To begin investigating the mechanisms of augmented anti-bacterial trained immunity, we examined kinetic chemokine responses in the lung. Thus, naive and 4-week viral-exposed BALB/c mice were infected with *S. pneumoniae* and chemokines were measured at various time points. Since memory AMs are marked by their increased *ex vivo* MIP-2 and KC production (Figures 1J, 2G, and 3C), we examined MIP-2 and KC along with four other inflammatory cytokines. The levels of MIP-2 and KC increased in lung tissues of viral-exposed mice by 12 hr, peaked by 24 hr, and declined by 48 hr (Ad), whereas they did not markedly increase until 48 hr in PBS animals (Figure 6A). Similar kinetics were observed with IP-10, MCP-1, MIP-1α, and IL-1β (Figure 6A). Given the accelerated cytokine responses in the lung, we examined kinetic responses of neutrophils and AMs that are critical for host defense against extracellular bacteria (Eddens and Kolls, 2012). Before bacterial infection (0 hr), both PBS and 4-week viral-exposed lungs (BAL and lung) had few neutrophils (Figure 6B), consistent with the lack of chemokines (Figure 6A). Upon bacterial infection, consistent with accelerated neutrophil chemokine responses in the lung of viral-exposed animals (Figure 6A), the numbers of neutrophils were much greater, particularly at 12 hr, both in BAL and lung of these mice than in PBS control (Figure 6B), while numbers of AMs were largely comparable between the two groups (Figure 6C). The ability of AMs to phagocytose and kill *S. pneumoniae* did not differ (Figure S7A and S7B).

The above data suggest a central role for accelerated neutrophilia in augmented anti-bacterial trained immunity in viral-exposed animals. To investigate this further, using a neutrophil-depleting mAb (αLy6G) or an isotype control Ab (Figure 6D), we partially or completely depleted neutrophils (Figure 6E) *in vivo* immediately after bacterial challenge in viral-exposed mice. Partial neutrophil depletion permitted to adequately address if accelerated and increased neutrophil responses in viral-exposed mice accounted for enhanced innate immunity. Compared to isotype Ab controls, the mice partially depleted of neutrophils (αLy6G 100 μg) had significantly reduced protection in the lung as shown by increased illness scores and bacterial counts (Figure 6F). Complete neutrophil depletion (αLy6G 200 μg) resulted in further worsened protection (Figure 6F). These data suggest that trained immunity in viral-exposed lungs enhances anti-bacterial protection via accelerated chemokine responses and tissue neutrophilia.

Memory AMs Exert Anti-bacterial Trained Immunity via Inducing Neutrophil Chemokine and Chemotaxis

To investigate the relationship between memory AMs, neutrophils, and protective innate immunity, we purified $CD11b^+$ or

Figure 5. Memory AM Are Associated with Long-Lasting Trained Immunity against Bacterial Infection

(A) Schema of intratracheal (i.t.) *S. pneumoniae* infection model in viral-exposed BALB/c mice.
(B) Survival of 4 weeks PBS or viral-exposed mice post-bacterial infection.
(C) Changes in illness score and body weight at 24, 48, and 72 hr post-bacterial infection.
(D) Bacterial counts (CFU) in the lung/spleen at 24, 48, 72 hr post-bacterial infection.
(E) Lung histopathologic images at 0, 24, 48, and 72 hr post-bacterial challenge. Scale bars: 500 μm
(F) Bacterial CFU in the lung/spleen of *S. pneumoniae*-infected BALB/c mice at 6, 8, or 16 weeks post-viral exposure.
(G) Schema of *S. pneumoniae* infection model in viral-exposed C57BL/6 mice.
(H) Bacterial CFU in the lung/spleen at 48 hr post-bacterial infection in 4 week viral-exposed C57BL/6 mice.
(I) Schema of *E. coli* infection model in viral-exposed BALB/c mice.
(J) Bacterial CFU in the lung at 8 and 24 hr post-*E. coli* infection in 4 week viral-exposed BALB/c mice.
Bar graphs are presented as mean ± SEM. Data are representative of two independent experiments (n = 5 mice/group except B where n = 10 mice/group). *$p < 0.05$; **$p < 0.01$.
See also Figure S6.

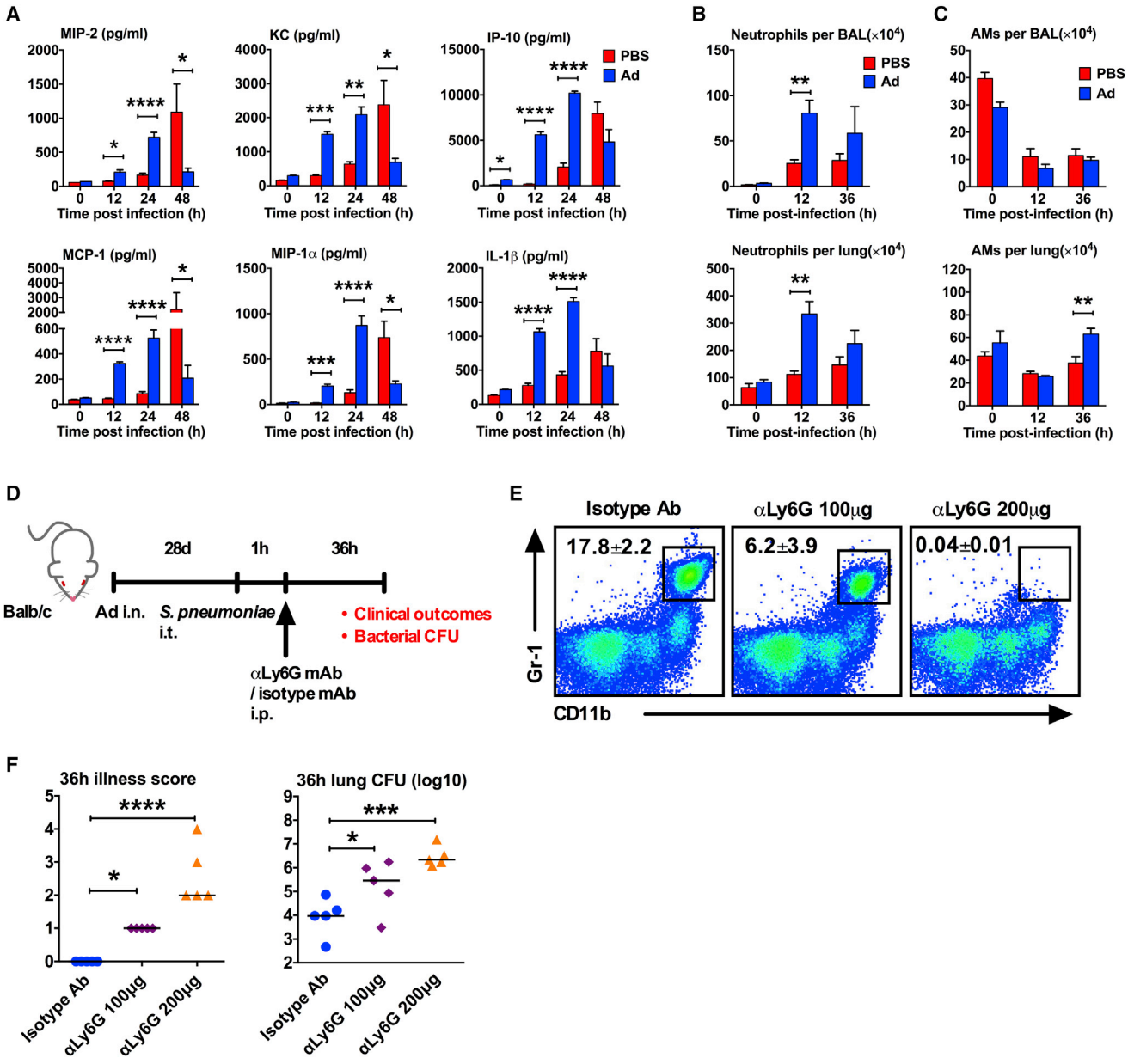

Figure 6. Trained Immunity Augments Anti-bacterial Protection via Accelerated Chemokine Responses and Neutrophilia in the Lung

(A) Levels of MIP-2, KC, and inflammatory cytokines in lung tissues at 0, 12, 24, and 48 hr post-bacterial infection in 4 week PBS or viral-exposed BALB/c mice.

(B) Numbers of neutrophils in BAL and lungs at 0, 12, and 36 hr post-bacterial infection in 4 week PBS or viral-exposed mice.

(C) Numbers of AM in BAL and lungs at 0, 12, and 36 hr post-bacterial infection in 4 week PBS or viral-exposed mice.

(D) Schema of neutrophil depletion in *S. pneumoniae*-infected BALB/c mice post-4 weeks viral exposure. Neutrophils were depleted by i.p. injection of anti-Ly6G or control mAb shortly after bacterial infection.

(E) Dotplots showing anti-Ly6G mAb dose-dependent neutrophil depletion in the blood.

(F) Illness scores and bacterial CFU in 36 hr bacterial-infected mice with or without neutrophil depletion with two doses of anti-Ly6G mAb.

Bar graphs are presented as mean ± SEM. Numbers in (E) are mean ± SD of % neutrophils in total blood leukocytes. Horizontal lines in (F) are median values. Data are representative of two independent experiments (n = 5 mice/group). *p < 0.05; **p < 0.01; ***p < 0.001; ****p < 0.0001.

See also Figure S7.

CD11c$^+$ innate immune cells from the lung tissue of 4-week viral-exposed mice and compared their *ex vivo* chemokine production and protective capacities upon *in vivo* transfer to naive mice (Figure 7A). Since AMs reside only within the CD11c$^+$, but not CD11b$^+$, cell population (Figure S1B), this approach allowed us to compare memory AMs with other macrophage populations in viral-exposed lungs in their relative roles in trained immunity. Upon bacterial stimulation and comparison with the cells from

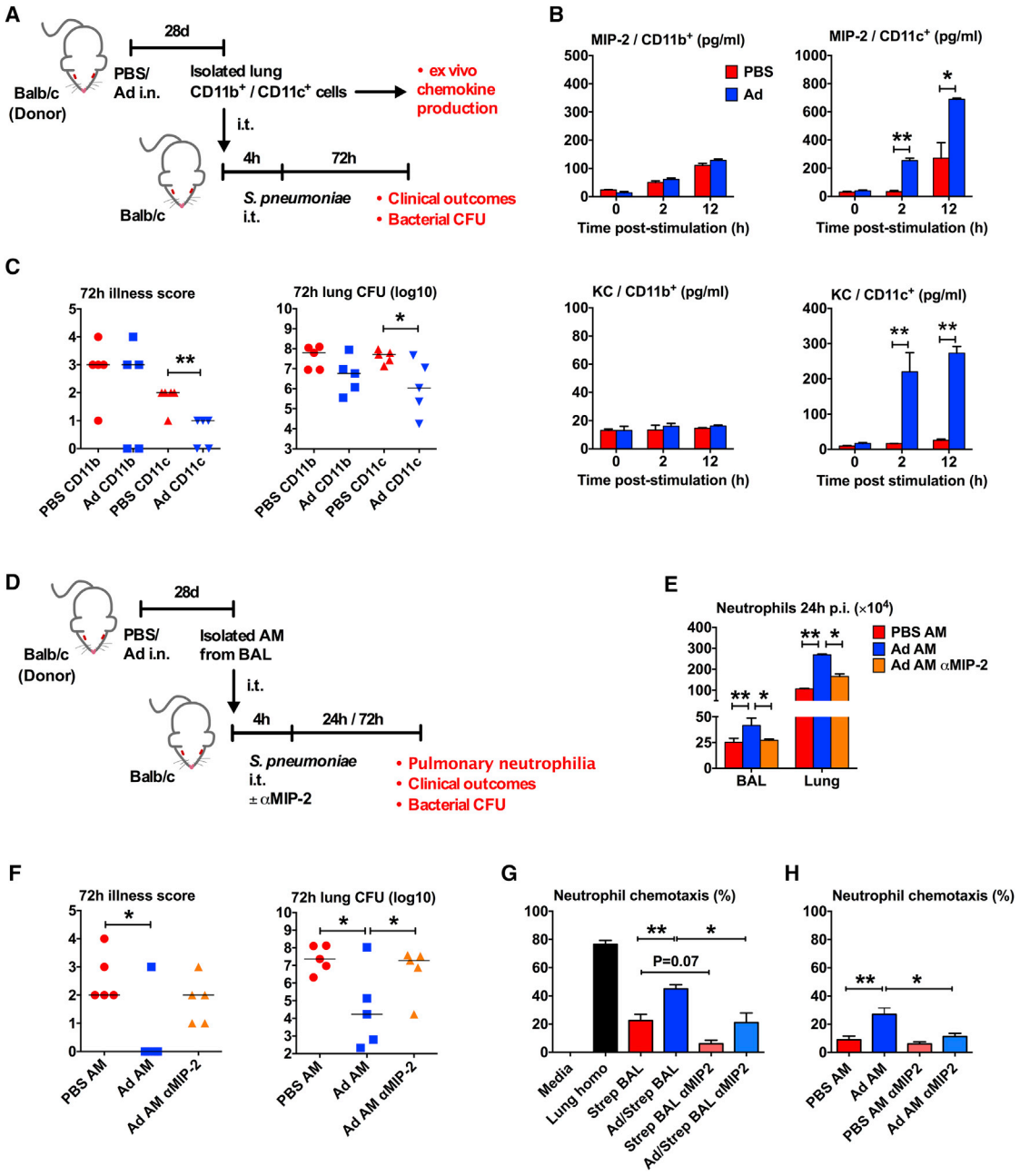

Figure 7. Memory AM Exert Anti-bacterial Trained Immunity via Inducing Neutrophil Chemokine and Chemotaxis

(A) Schema of evaluating roles of CD11b$^+$ or CD11c$^+$ cells in the lung of day 28 PBS or viral-exposed donor BALB/c mice. Cells were isolated and *ex vivo* stimulated for chemokine analysis, or transferred i.t. to the lung of naive mice for protection analysis post-*S. pneumoniae* infection.

(B) MIP-2 and KC contents in supernatants of *S. pneumoniae*-stimulated CD11b$^+$ or CD11c$^+$ innate immune cells.

(C) Illness scores and bacterial CFU at 72 hr post-bacterial infection of naive BALB/c mice transferred i.t. with CD11b$^+$ or CD11c$^+$ cells from day 28 viral-exposed donor mice.

(D) Schema of evaluating roles of AM isolated from the airway of day 28 PBS or viral-exposed donor BALB/c mice. AM were transferred i.t. to the airway of naive BALB/c mice for protection analysis. Shortly after bacterial challenge, some mice were injected with anti-MIP-2 Abs.

(E) Numbers of neutrophils at 24 hr post-bacterial infection in mice with transferred AM and with or without *in vivo* MIP-2 neutralization.

(F) Illness scores and bacterial CFU of 72-hr bacterial-infected mice with transferred AM and with or without *in vivo* MIP-2 neutralization.

(legend continued on next page)

naive lungs, the CD11c$^+$ cells, but not CD11b$^+$ cells, of viral-exposed lungs produced increased MIP-2 and KC (Figure 7B). Of importance, only the CD11c$^+$ cells from viral-exposed animals, but not CD11c$^+$ cells from PBS animals, transferred into the airway of naive recipient animals, provided enhanced anti-bacterial protection (Figure 7C). On the other hand, CD11b$^+$ cells, whether from viral-exposed or naive animals, failed to enhance protection (Figure 7C). These data suggest that memory AMs, but not other macrophage subsets, in the lung of viral-exposed animals mediate anti-bacterial trained immunity via enhanced neutrophil chemokine production.

As CD11c$^+$ cells transferred as described above might contain dendritic cells, to further determine the relationship of memory AM to neutrophils and anti-bacterial protection *in vivo*, we purified AMs directly from the airway (BAL) of PBS control (PBS AM) and 4-week viral-exposed (Ad AM) mice and transferred to the airway of naive mice (Figure 7D). Mice were then challenged with *S. pneumoniae*. Another group of Ad AM mice was injected with anti-MIP-2 Abs for chemokine blockade (Ad AM αMIP-2). Mice engrafted with AMs from naive mice (PBS AM) had some neutrophils in the lung and showed high illness scores and bacterial infection in the lung (Figures 7E and 7F). In contrast, animals engrafted with AMs from viral-exposed mice (Ad AM) had significantly more neutrophils in the BAL and lung in response to bacterial infection (Figure 7E), which was associated with much enhanced protection (Figure 7F). However, blockade of MIP-2 (Ad AM αMIP-2) drastically reduced neutrophils and anti-bacterial protection (Figures 7E and 7F). These data establish a direct relationship between airway memory AMs, neutrophilia, and trained immunity *in vivo*.

We next used *ex vivo* neutrophil chemotaxis assay to demonstrate the direct effect of memory AM-derived MIP-2 on neutrophil chemotaxis. Compared to the BAL fluids from *S. pneumoniae*-infected naive PBS mice (Strep BAL), the BAL from viral-exposed mice (Ad/Strep BAL) induced significantly greater neutrophil chemotaxis (Figure 7G). However, neutralization of MIP-2 in Ad/Strep BAL markedly reduced it (Figure 7G). Furthermore, compared to the AMs from naive animals (PBS AM), culture supernatants of memory AMs from viral-exposed mice (Ad AM) induced greater neutrophil chemotaxis, whereas MIP-2 neutralization reduced it (Ad AM αMIP-2) (Figure 7H). Together, the above data indicate that memory AMs play a critical role in anti-bacterial trained immunity via enhanced chemokine responses and neutrophil chemotaxis.

DISCUSSION

Immunological memory has long been ascribed only to adaptive T and B cells (Farber et al., 2016). The recently emerged concept of innate immune memory or trained immunity is defined as a reset persisting homeostatic state of innate immune cells following the resolution of a primary infection, leading to subsequently enhanced nonspecific responsiveness to the same or unrelated pathogens (Gourbal et al., 2018; Hamon and Quintin, 2016). To date, innate immune memory has mostly been studied as systemically acquired in settings of parenteral infection or vaccination. Thus, induction and mechanisms of innate immune memory in local tissues remain a priority of investigation (Chen et al., 2014; Gourbal et al., 2018; Wendeln et al., 2018). The knowledge in innate memory of mucosal macrophages is particularly lacking. Although innate immune memory shares some features with adaptive immunity, the relationship between adaptive immunity and innate immune memory remains unknown. Here, we show that acute respiratory viral infection induces memory AMs with sustained changes in surface markers, gene expression, metabolism, and anti-microbial responsiveness. Such memory AMs self-sustain via low-rate proliferation independently of circulating monocytes. Of importance, the priming of memory AM requires the help from effector CD8 T cells homed to the respiratory mucosa in the early stage of anti-viral responses.

Our study establishes a new paradigm of immunological memory formation by showing a previously unrecognized mechanistic link between adaptive immunity and innate immune memory. Different from the classical immunological memory development whereby activated innate APC trigger adaptive memory T cell formation, this paradigm suggests that adaptive immune cells such as T cells can reciprocally interact with innate macrophages on the mucosal surface to trigger macrophage memory development. This pathway may have resulted from a co-evolutionary process of innate and adaptive immune systems in vertebrates where they benefit from triggering each other's memory acquisition. In so doing, the mucosal sites are protected not only from the initially encountered pathogen but also from other pathogens. Our study further reveals the requirement of T cells for the priming, but not maintenance, of memory AMs. Such a jump-start of memory macrophage formation by effector T cells is reminiscent of the "jump-start" nature of memory T cell differentiation upon a brief encounter of naive Ag-specific T cells with APC (Kaech and Ahmed, 2001). Thus, the novel function of T cells identified by us, together with their known functions, suggests that Ag-specific T cells may participate in host defense via their Ag-dependent macrophage activation (Eddens and Kolls, 2012), "innate-like" immune activities (Berg et al., 2003; Strutt et al., 2010), and priming of memory macrophages. We further find effector T cell-derived IFN-γ to be critical to prime for memory AMs, which adds to the importance of IFN-γ in trained immunity as this cytokine is also involved in training myeloid progenitors in the bone marrow (Kaufmann et al., 2018). Future studies shall address if memory AMs develop after exposure to other respiratory pathogens and if T cells prime for innate immune memory in other tissues. The effect of T cell-derived IFN-γ on macrophages is likely contextual since one mechanism by which flu impairs innate

(G) *Ex vivo* neutrophil chemotaxis by tissue homogenates (homo) and bronchoalveolar lavage (BAL) from bacterial-infected or bacterial infected-viral exposed lungs with or without *in vitro* MIP-2 neutralization.

(H) *Ex vivo* neutrophil chemotaxis by bacterial-stimulated AM supernatants with or without *in vitro* MIP-2 neutralization.

Horizontal lines in scatter dotplots are median values. Bar graphs are presented as mean ± SD. Data are representative of two independent experiments (B, C, E, and F: n = 5 mice/group; G and H: 3 wells/group). *$p < 0.05$; **$p < 0.01$.

immunity is via IFN-γ-mediated macrophage tolerance in the lung (Sun and Metzger, 2008).

Our findings also suggest that exposure to less virulent viruses such as adenoviruses, which usually cause only a mild cold in humans, is beneficial to the host via generating both Ag-specific T/B cell immunity and non-specific, broadly protective memory macrophages. In keeping with the currently understood trait of innate memory cells (Gourbal et al., 2018; Netea et al., 2016), we find memory AMs not to constitutively produce inflammatory mediators unless they encounter danger signals. Moreover, memory AMs, like naive AMs, undergo only low-grade proliferation to maintain itself. These all are to ensure the lung to remain inflammation-free after returning to homeostasis post-viral infection. It also helps maintain the dual regulatory and inflammatory property of AMs in an organ with a vital gas-exchange function (Hussell and Bell, 2014). The "homeostatic" status of memory AMs is likely attributed to the transient nature of adenoviral infection. This is different from chronic nature of herpes viral infection, which also induces persisting changes in systemic or local macrophages (Barton et al., 2007; Machiels et al., 2017), but such an altered innate immune state is not deemed as bona fide innate memory (Hamon and Quintin, 2016). Based on our data and those from others, it is plausible to propose that while memory macrophages at mucosal sites are beneficial to host defense, those in non-mucosal tissues such as the brain (Wendeln et al., 2018) and vasculature (Groh et al., 2018) could be pathogenic.

Most of the current knowledge in innate immune memory is drawn from settings of systemic infection or immunization, which induces systemically acquired innate memory in circulating monocytes or macrophages (Arts et al., 2018; Kaufmann et al., 2018; Mitroulis et al., 2018). Such systemic innate memory involves trained myeloid progenitors in the bone marrow (Kaufmann et al., 2018; Mitroulis et al., 2018). In contrast, we show that mucosally induced memory macrophages do not involve BM progenitors and blood monocytes. We observed a contribution of circulating monocytes to the memory AM pool only when the endogenous (recipient-derived) AM population in BM chimera was impaired by irradiation, in accord with the current knowledge (Guilliams et al., 2013b; Hashimoto et al., 2013). Thus, the autonomous nature of memory AMs on the mucosal surface demonstrated by us suggests that innate immune memory may arise and sustain locally from long-lived residential macrophages as long as the initiating insult does not severely diminish the population size. We believe that such unique tissue-restricted innate memory has advantages over systemically acquired innate memory in that it will not cause a globally imprinted immunological bias, which may not always be beneficial to the host.

Our study fosters developing novel vaccine strategies (Blok et al., 2015; Jeyanathan et al., 2018), as most current vaccine strategies only aim to induce Ag-specific adaptive immune memory cells. Effective strategies, including mucosal vaccination, should induce both innate and adaptive memory responses against not only the targeted but un-related pathogens.

STAR★METHODS

Detailed methods are provided in the online version of this paper and include the following:

SUPPLEMENTAL INFORMATION

Supplemental Information includes seven figures and three tables and can be found with this article online at https://doi.org/10.1016/j.cell.2018.09.042.

ACKNOWLEDGMENTS

The work was supported by the Foundation and other grant programs of the Canadian Institutes of Health Research (FDN#154316, FRN#148567, MOP-14181, CPG-127775), Natural Sciences and Engineering Research Council of Canada (FRN#319834), and Ontario Thoracic Society. We thank Xueya Feng, Anna Zganiacz, Shreya Jain, Danya Thayaparan, Caleb Zavitz, and Shaun Pacheco for technical support and Dr. Cory Hogaboam for providing anti-MIP-2 serum.

AUTHOR CONTRIBUTIONS

Y.Y., M.J., and Z.X. conceived and designed the study. Y.Y., M.J., S.H., N.G.B., M.V.-S., D.D., R.L., S.A., and Y.C. performed experiments. C.S.R. and J.D.S. supervised parabiosis or metabolism analysis. Y.Y., M.J., N.G.B., and A.D.-G. analyzed data. Y.Y. and Z.X. wrote the paper.

DECLARATION OF INTERESTS

The authors declare no competing interests.

Received: May 6, 2018
Revised: August 20, 2018
Accepted: September 19, 2018
Published: October 25, 2018

REFERENCES

Arts, R.J.W., Moorlag, S.J.C.F.M., Novakovic, B., Li, Y., Wang, S.-Y., Oosting, M., Kumar, V., Xavier, R.J., Wijmenga, C., Joosten, L.A.B., et al. (2018). BCG Vaccination Protects against Experimental Viral Infection in Humans through the Induction of Cytokines Associated with Trained Immunity. Cell Host Microbe *23*, 89–100.

Barton, E.S., White, D.W., Cathelyn, J.S., Brett-McClellan, K.A., Engle, M., Diamond, M.S., Miller, V.L., and Virgin, H.W., 4th. (2007). Herpesvirus latency confers symbiotic protection from bacterial infection. Nature *447*, 326–329.

Bassett, J.D., Yang, T.C., Bernard, D., Millar, J.B., Swift, S.L., McGray, A.J.R., VanSeggelen, H., Boudreau, J.E., Finn, J.D., Parsons, R., et al. (2011). CD8+ T-cell expansion and maintenance after recombinant adenovirus immunization rely upon cooperation between hematopoietic and nonhematopoietic antigen-presenting cells. Blood *117*, 1146–1155.

Berg, R.E., Crossley, E., Murray, S., and Forman, J. (2003). Memory CD8+ T cells provide innate immune protection against Listeria monocytogenes in the absence of cognate antigen. J. Exp. Med. *198*, 1583–1593.

Blok, B.A., Arts, R.J.W., van Crevel, R., Benn, C.S., and Netea, M.G. (2015). Trained innate immunity as underlying mechanism for the long-term, nonspecific effects of vaccines. J. Leukoc. Biol. *98*, 347–356.

Chen, F., Wu, W., Millman, A., Craft, J.F., Chen, E., Patel, N., Boucher, J.L., Urban, J.F.J., Jr., Kim, C.C., and Gause, W.C. (2014). Neutrophils prime a long-lived effector macrophage phenotype that mediates accelerated helminth expulsion. Nat. Immunol. *15*, 938–946.

Cheng, S.-C., Quintin, J., Cramer, R.A., Shepardson, K.M., Saeed, S., Kumar, V., Giamarellos-Bourboulis, E.J., Martens, J.H.A., Rao, N.A., Aghajanirefah, A., et al. (2014). mTOR- and HIF-1α-mediated aerobic glycolysis as metabolic basis for trained immunity. Science *345*, 1250684.

Damjanovic, D., Lai, R., Jeyanathan, M., Hogaboam, C.M., and Xing, Z. (2013). Marked improvement of severe lung immunopathology by influenza-associated pneumococcal superinfection requires the control of both bacterial replication and host immune responses. Am. J. Pathol. *183*, 868–880.

Didierlaurent, A., Goulding, J., Patel, S., Snelgrove, R., Low, L., Bebien, M., Lawrence, T., van Rijt, L.S., Lambrecht, B.N., Sirard, J.-C., and Hussell, T. (2008). Sustained desensitization to bacterial Toll-like receptor ligands after resolution of respiratory influenza infection. J. Exp. Med. *205*, 323–329.

Eddens, T., and Kolls, J.K. (2012). Host defenses against bacterial lower respiratory tract infection. Curr. Opin. Immunol. *24*, 424–430.

Ensan, S., Li, A., Besla, R., Degousee, N., Cosme, J., Roufaiel, M., Shikatani, E.A., El-Maklizi, M., Williams, J.W., Robins, L., et al. (2016). Self-renewing resident arterial macrophages arise from embryonic CX3CR1(+) precursors and circulating monocytes immediately after birth. Nat. Immunol. *17*, 159–168.

Epelman, S., Lavine, K.J., and Randolph, G.J. (2014). Origin and functions of tissue macrophages. Immunity *41*, 21–35.

Farber, D.L., Netea, M.G., Radbruch, A., Rajewsky, K., and Zinkernagel, R.M. (2016). Immunological memory: lessons from the past and a look to the future. Nat. Rev. Immunol. *16*, 124–128.

Gomez Perdiguero, E., Klapproth, K., Schulz, C., Busch, K., Azzoni, E., Crozet, L., Garner, H., Trouillet, C., de Bruijn, M.F., Geissmann, F., and Rodewald, H.R. (2015). Tissue-resident macrophages originate from yolk-sac-derived erythro-myeloid progenitors. Nature *518*, 547–551.

Gourbal, B., Pinaud, S., Beckers, G.J.M., Van Der Meer, J.W.M., Conrath, U., and Netea, M.G. (2018). Innate immune memory: An evolutionary perspective. Immunol. Rev. *283*, 21–40.

Groh, L., Keating, S.T., Joosten, L.A.B., Netea, M.G., and Riksen, N.P. (2018). Monocyte and macrophage immunometabolism in atherosclerosis. Semin. Immunopathol. *40*, 203–214.

Guilliams, M., Lambrecht, B.N., and Hammad, H. (2013a). Division of labor between lung dendritic cells and macrophages in the defense against pulmonary infections. Mucosal Immunol. *6*, 464–473.

Guilliams, M., De Kleer, I., Henri, S., Post, S., Vanhoutte, L., De Prijck, S., Deswarte, K., Malissen, B., Hammad, H., and Lambrecht, B.N. (2013b). Alveolar macrophages develop from fetal monocytes that differentiate into long-lived cells in the first week of life via GM-CSF. J. Exp. Med. *210*, 1977–1992.

Hamon, M.A., and Quintin, J. (2016). Innate immune memory in mammals. Semin. Immunol. *28*, 351–358.

Hashimoto, D., Chow, A., Noizat, C., Teo, P., Beasley, M.B., Leboeuf, M., Becker, C.D., See, P., Price, J., Lucas, D., et al. (2013). Tissue-resident macrophages self-maintain locally throughout adult life with minimal contribution from circulating monocytes. Immunity *38*, 792–804.

Hoeffel, G., Chen, J., Lavin, Y., Low, D., Almeida, F.F., See, P., Beaudin, A.E., Lum, J., Low, I., Forsberg, E.C., et al. (2015). C-Myb(+) erythro-myeloid progenitor-derived fetal monocytes give rise to adult tissue-resident macrophages. Immunity *42*, 665–678.

Hussell, T., and Bell, T.J. (2014). Alveolar macrophages: plasticity in a tissue-specific context. Nat. Rev. Immunol. *14*, 81–93.

Jeyanathan, M., Mu, J., McCormick, S., Damjanovic, D., Small, C.-L., Shaler, C.R., Kugathasan, K., and Xing, Z. (2010). Murine airway luminal antituberculosis memory CD8 T cells by mucosal immunization are maintained via antigen-driven in situ proliferation, independent of peripheral T cell recruitment. Am. J. Respir. Crit. Care Med. *181*, 862–872.

Jeyanathan, M., Afkhami, S., Khera, A., Mandur, T., Damjanovic, D., Yao, Y., Lai, R., Haddadi, S., Dvorkin-Gheva, A., Jordana, M., et al. (2017). CXCR3 Signaling Is Required for Restricted Homing of Parenteral Tuberculosis Vaccine-Induced T Cells to Both the Lung Parenchyma and Airway. J. Immunol. *199*, 2555–2569.

Jeyanathan, M., Yao, Y., Afkhami, S., Smaill, F., and Xing, Z. (2018). New Tuberculosis Vaccine Strategies: Taking Aim at Un-Natural Immunity. Trends Immunol. *39*, 419–433.

Kaech, S.M., and Ahmed, R. (2001). Memory CD8+ T cell differentiation: initial antigen encounter triggers a developmental program in naïve cells. Nat. Immunol. *2*, 415–422.

Kaufmann, E., Sanz, J., Dunn, J.L., Khan, N., Mendonça, L.E., Pacis, A., Tzelepis, F., Pernet, E., Dumaine, A., Grenier, J.-C., et al. (2018). BCG Educates Hematopoietic Stem Cells to Generate Protective Innate Immunity against Tuberculosis. Cell *172*, 176–190.

Kohlmeier, J.E., and Woodland, D.L. (2009). Immunity to respiratory viruses. Annu. Rev. Immunol. *27*, 61–82.

Low, N., Bavdekar, A., Jeyaseelan, L., Hirve, S., Ramanathan, K., Andrews, N.J., Shaikh, N., Jadi, R.S., Rajagopal, A., Brown, K.E., et al. (2015). A randomized, controlled trial of an aerosolized vaccine against measles. N. Engl. J. Med. *372*, 1519–1529.

Machiels, B., Dourcy, M., Xiao, X., Javaux, J., Mesnil, C., Sabatel, C., Desmecht, D., Lallemand, F., Martinive, P., Hammad, H., et al. (2017). A gammaherpesvirus provides protection against allergic asthma by inducing the replacement of resident alveolar macrophages with regulatory monocytes. Nat. Immunol. *18*, 1310–1320.

Misharin, A.V., Morales-Nebreda, L., Mutlu, G.M., Budinger, G.R.S., and Perlman, H. (2013). Flow cytometric analysis of macrophages and dendritic cell subsets in the mouse lung. Am. J. Respir. Cell Mol. Biol. *49*, 503–510.

Mitroulis, I., Ruppova, K., Wang, B., Chen, L.-S., Grzybek, M., Grinenko, T., Eugster, A., Troullinaki, M., Palladini, A., Kourtzelis, I., et al. (2018). Modulation of Myelopoiesis Progenitors Is an Integral Component of Trained Immunity. Cell *172*, 147–161.

Netea, M.G., Joosten, L.A.B., Latz, E., Mills, K.H.G., Natoli, G., Stunnenberg, H.G., O'Neill, L.A.J., and Xavier, R.J. (2016). Trained immunity: A program of innate immune memory in health and disease. Science *352*, aaf1098.

Sabatel, C., Radermecker, C., Fievez, L., Paulissen, G., Chakarov, S., Fernandes, C., Olivier, S., Toussaint, M., Pirottin, D., Xiao, X., et al. (2017). Exposure

to Bacterial CpG DNA Protects from Airway Allergic Inflammation by Expanding Regulatory Lung Interstitial Macrophages. Immunity *46*, 457–473.

Smaill, F., Jeyanathan, M., Smieja, M., Medina, M.F., Thanthrige-Don, N., Zganiacz, A., Yin, C., Heriazon, A., Damjanovic, D., Puri, L., et al. (2013). A human type 5 adenovirus-based tuberculosis vaccine induces robust T cell responses in humans despite preexisting anti-adenovirus immunity. Sci. Transl. Med. *5*, 205ra134.

Strutt, T.M., McKinstry, K.K., Dibble, J.P., Winchell, C., Kuang, Y., Curtis, J.D., Huston, G., Dutton, R.W., and Swain, S.L. (2010). Memory CD4+ T cells induce innate responses independently of pathogen. Nat. Med. *16*, 558–564, 1p following 564.

Sun, K., and Metzger, D.W. (2008). Inhibition of pulmonary antibacterial defense by interferon-gamma during recovery from influenza infection. Nat. Med. *14*, 558–564.

Wendeln, A.-C., Degenhardt, K., Kaurani, L., Gertig, M., Ulas, T., Jain, G., Wagner, J., Häsler, L.M., Wild, K., Skodras, A., et al. (2018). Innate immune memory in the brain shapes neurological disease hallmarks. Nature *556*, 332–338.

Xing, Z., Zganiacz, A., Wang, J., Divangahi, M., and Nawaz, F. (2000). IL-12-independent Th1-type immune responses to respiratory viral infection: requirement of IL-18 for IFN-gamma release in the lung but not for the differentiation of viral-reactive Th1-type lymphocytes. J. Immunol. *164*, 2575–2584.

Yao, Y., Lai, R., Afkhami, S., Haddadi, S., Zganiacz, A., Vahedi, F., Ashkar, A.A., Kaushic, C., Jeyanathan, M., and Xing, Z. (2017). Enhancement of Antituberculosis Immunity in a Humanized Model System by a Novel Virus-Vectored Respiratory Mucosal Vaccine. J. Infect. Dis. *216*, 135–145.

STAR★METHODS

KEY RESOURCES TABLE

REAGENT or RESOURCE	SOURCE	IDENTIFIER
Antibodies		
Anti-mouse CD45 APC-Cy7 (clone 30-F11)	BD Biosciences	Cat# 557659; RRID:AB_396774
Anti-mouse CD11b PE-Cy7 (clone M1/70)	BD Biosciences	Cat# 552850; RRID:AB_394491
Anti-mouse CD11c APC (clone HL3)	BD Biosciences	Cat# 550261; RRID:AB_398460
Anti-mouse CD11c BV711 (clone HL3)	BD Biosciences	Cat#563048; PRID:AB_2734778
Anti-mouse MHC II AF700 (clone M5/114.15.2)	Thermo Fisher Scientific	Cat# 56-5321-82; RRID:AB_494009
Anti-mouse CD3 V450 (clone 17A2)	BD Biosciences	Cat# 561389; RRID:AB_10679120
Anti-mouse CD45R V450 (clone RA3-6B2)	BD Biosciences	Cat# 560473; RRID:AB_1645277
Anti-mouse Ly6C Biotin (clone HK1.4)	BioLegend	Cat# 128003
Streptavidin Qdot800	Thermo Fisher Scientific	Cat# Q10173MP
Anti-mouse CD24 BV650 (clone M1/69)	BD Biosciences	Cat# 563545; PRID:AB_2738271
Anti-mouse CD64 PE (clone X54-5/7.1)	BioLegend	Cat# 139303; RRID:AB_10613467
Anti-mouse Ly6G BV605 (clone 1A8)	BD Biosciences	Cat# 563005; PRID:AB_2737946
Anti-mouse Siglec-F PE-CF594 (clone E50-2440)	BD Biosciences	Cat# 562757; RRID:AB_2687994
Anti-mouse CD80 PerCP-Cy5.5 (clone 16-10A1)	BD Biosciences	Cat# 560526; RRID:AB_1727514
Anti-mouse CD86 V450 (clone GL1)	BD Biosciences	Cat# 560450; RRID:AB_1645280
Anti-mouse CD284 APC (clone SA15-21)	BioLegend	Cat# 145405; RRID:AB_2562502
Anti-mouse CD282 BV421 (clone CB225)	BD Biosciences	Cat# 565908; PRID:AB_2739387
Anti-mouse CD192 BV421 (clone SA203G11)	BioLegend	Cat# 150605; RRID:AB_2571913
Anti-mouse CD4 PE-Cy7 (clone RM4-5)	BD Biosciences	Cat# 552775; RRID:AB_394461
Anti-mouse CD8 APC-Cy7 (clone 53-6.7)	BD Biosciences	Cat# 557654; PRID:AB_396769
Anti-mouse IFN-γ APC (clone XMG1.2)	BD Biosciences	Cat# 554413
Anti-mouse CD45.2 PerCP-Cy5.5 (clone 104)	BD Biosciences	Cat# 552950; RRID:AB_394528
Anti-mouse CD45.1 APC-Cy7 (clone A20)	BD Biosciences	Cat# 560579; RRID:AB_1727487
Anti-mouse Ki-67 BV421 (clone 16A8)	BD Biosciences	Cat# 652411; RRID:AB_2562663
Anti-BrdU APC (clone B44)	BD Biosciences	Cat# 51-23619L
Purified Rat Anti-Mouse CD16/CD32 (clone 2.4G2)	BD BioSciences	Cat# 553141; RRID:AB_394656
Purified anti-mouse Ly6G (clone 1A8)	UCSF Monoclonal Antibody Core	Cat# AM050 https://antibodies.ucsf.edu/antibody-ordering-catalog
Rat IgG2a isotype Ab (clone 2A3)	BioXCell	Cat# BE0089
Purified anti-mouse CD4 (clone GK1.5)	Dr. Zhou Xing Mcmaster University, Hamilton, Canada	N/A
Purified anti-mouse CD8 (clone 2.43)	Dr. Zhou Xing Mcmaster University, Hamilton, Canada	N/A
Rabbit anti-murine MIP-2 polyclonal Ab	Dr. Cory M. Hogaboam University of Michigan, Ann Arbor, USA	(Damjanovic et al., 2013)
Normal rabbit serum	Dr. Cory M. Hogaboam University of Michigan, Ann Arbor, USA	(Damjanovic et al., 2013)

(*Continued on next page*)

Continued

REAGENT or RESOURCE	SOURCE	IDENTIFIER
Bacterial and Virus Strains		
Human serotype 5 adenovirus (wild type Ad)	Dr. Zhou Xing McMaster University, Hamilton, ON, Canada	(Xing et al., 2000)
Recombinant human serotype 5 adenovirus expressing *M.tb* Antigen 85A (AdHu5Ag85A)	Dr. Zhou Xing McMaster University, Hamilton, ON, Canada	(Smaill et al., 2013)
Streptococcus pneumoniae	ATCC	ATCC Number: 6303
Escherichia coli	ATCC	ATCC Number: 25922
Biological Samples		
Tryptic soy agar	BD Biosciences	Cat# 236950
Defibrinated sheep blood	Hemostat	Cat# DSB100
Neomycin sulfate	Sigma-Aldrich	CAS Number: 1405-10-3
Todd Hewitt broth	BD Biosciences	Cat# 249240
Tryptic soy broth	BD Biosciences	Cat# 211825
Collagenase type I	ThermoFisher Scientific	Cat# 17100-017
ACK lysing buffer	ThermoFisher Scientific	Cat# A10492-01
FBS	ThermoFisher Scientific	Cat# 16140071
BSA	Sigma-Aldrich	Cat# 10735086001
Penicillin-Streptomycin	ThermoFisher Scientific	Cat# 15140122
L-Glutamine	ThermoFisher Scientific	Cat# A2916801
HBSS	ThermoFisher Scientific	Cat# 14185-052
MEM Non-Essential Amino Acids Solution	ThermoFisher Scientific	Cat# 11140076
HEPES	ThermoFisher Scientific	Cat# 15630080
Sodium Pyruvate	ThermoFisher Scientific	Cat# 11360070
2-Mercaptoethanol	ThermoFisher Scientific	Cat# 21985023
PerColl	Sigma-Aldrich	Cat# 17-0891-02
Turk blood diluting fluid	RICCA Chemical	Cat# 8850-16
Seahorse XF base medium	Agilent Technologies	Cat#102353-100
Seahorse XF Calibrant Solution	Agilent Technologies	Cat#100840-000
Chemicals, Peptides, and Recombinant Proteins		
Recombinant murine IFN-γ	Peprotech	315-05
Critical Commercial Assays		
Annexin V Apoptosis Detection Kit APC	ThermoFisher Scientific	Cat# 88-8007-72
Aqua dead cell staining kit	ThermoFisher Scientific	Cat# L34957
MILLIPLEX MAP Mouse Cytokine/Chemokine Magnetic Bead Panel - Immunology Multiplex Assay	Millipore Sigma	Cat# MCYTOMAG-70K
APC BrdU Flow Kit	BD Biosciences	Cat# 557892
RNeasy micro kit	QIAGEN	Cat# 74004
Mouse IL-1 beta DuoSet ELISA kit	R&D Systems	Cat# DY401-05
Mouse IFN-gamma DuoSet ELISA kit	R&D Systems	Cat# DY485-05
Seahorse XF Glycolysis Stress Test Kit	Agilent Technologies	Cat#103020-100
Deposited Data		
Raw RNA microarray data	Gene Expression Omnibus (GEO) database	GEO: GSE118512
Experimental Models: Organisms/Strains		
Mouse: BALB/cJ	The Jackson Laboratory	IMSR Cat# JAX:000651; RRID:IMSR_JAX:000651
Mouse: BALB/c	Charles River	IMSR Cat# CRL:547; RRID:IMSR_CRL:547
Mouse: C57BL/6J	The Jackson Laboratory	IMSR Cat# JAX:000664; RRID:IMSR_JAX:000664

(*Continued on next page*)

Continued

REAGENT or RESOURCE	SOURCE	IDENTIFIER
Mouse: B6.129S7-*Ifng*^{tm1Ts}/J	The Jackson Laboratory	IMSR Cat# JAX:002287; RRID:IMSR_JAX:002287
Mouse: B6.129S4-*Ccr2*^{tm1Ifc}/J	The Jackson Laboratory	IMSR Cat# JAX:004999; RRID:IMSR_JAX:004999
Mouse: B6.129S7-*Rag1*^{tm1Mom}/J	The Jackson Laboratory	IMSR Cat# JAX:002216; RRID:IMSR_JAX:002216
Mouse: CBySmn.CB17-*Prkdc*^{scid}/J	The Jackson Laboratory	IMSR Cat# JAX:001803; RRID:IMSR_JAX:001803
Mouse: CByJ.SJL(B6)-*Ptprc*^{a}/J	The Jackson Laboratory	IMSR Cat# JAX:006584; RRID:IMSR_JAX:006584
Mouse: B6.129S7-*Ifngr1*^{tm1Agt}/J	The Jackson Laboratory	IMSR Cat# JAX:003288; RRID:IMSR_JAX:003288
Mouse: B6.SJL-*Ptprc*^{a} *Pepc*^{b}/BoyJ	The Jackson Laboratory	IMSR Cat# JAX:002014; RRID:IMSR_JAX:002014
Software and Algorithms		
Openlab, version 5.0.2	Improvision, Coventry, UK	RRID: SCR_012158
xPONENT, version 4.2	ThermoFisher Scientific	https://www.luminexcorp.com/xponent/
GraphPad Prism, version 6	https://www.graphpad.com/scientific-software/prism/	RRID: SCR_002798
FlowJo, version 10	https://www.flowjo.com	RRID: SCR_008520
Wave Desktop, version 2.6	Agilent Technologies	https://www.agilent.com/en/products/cell-analysis/software-download-for-wave-desktop
Other		
CD11c MicroBeads, mouse	Miltenyi Biotech	Cat# 130-052-001
CD11b MicroBeads, human and mouse	Miltenyi Biotech	Cat# 130-049-601
Mouse CD8 T cell isolation kit	StemCell Technologies	Cat# 19853
CD3ε Microbead Kit, mouse	Miltenyi Biotech	Cat# 130-094-973
Clophosome and Control Liposomes	FormuMax Scientific	Cat# F70101C-NC

CONTACT FOR REAGENT AND RESOURCE SHARING

Further information and requests for resources and reagents should be directed to and will be fulfilled by the Lead Contact, Zhou Xing (xingz@mcmaster.ca).

EXPERIMENTAL MODEL AND SUBJECT DETAILS

Mice

Wild-type female BALB/c and C57BL/6 mice were purchased from Charles River Laboratories (Saint Constant, QC, Canada) or the Jackson Laboratory (Bar Harbor, ME). Female Interferon-γ (IFN-γ) knockout mice on a C57BL/6 background (B6.129S7-*Ifng*^{tm1Ts}/J), Interferon-γ receptor (IFN-γR) knockout mice on a C57BL/6 background (B6.129S7-*Ifngr1*^{tm1Agt}/J), Chemokine (C-C motif) receptor 2 (CCR2) knockout mice on a C57BL/6 background (B6.129S4-*Ccr2*^{tm1Ifc}/J), recombination activating gene 1 (Rag1) knockout mice on a C57BL/6 background (B6.129S7-*Rag1*^{tm1Mom}/J), SCID mice on a BALB/c background (CBySmn.CB17-*Prkdc*^{scid}/J), CD45.1 congenic mice on a BALB/cByJ background (CByJ.SJL(B6)-*Ptprc*^{a}/J), and CD45.1 congenic mice on a C57BL/6 background (B6.SJL-*Ptprc*^{a} *Pepc*^{b}/BoyJ) were all purchased from the Jackson Laboratory (Bar Harbor, ME). All mice were 6-8 week of age upon arrival. Mice were housed in a specific pathogen-free level B facility at McMaster University or University Health Network, Toronto. All experiments were carried out in accordance with the institutional guidelines from the Animal Research and Ethics Boards.

METHOD DETAILS

Respiratory infection by adenoviruses

Acute respiratory viral infection was elicited by using either a recombinant human serotype 5 adenovirus expressing an *Mtb* protein (Smaill et al., 2013) or a wild-type human serotype 5 adenovirus (Xing et al., 2000). The production and utilization of these viruses were previously described (Jeyanathan et al., 2010; Xing et al., 2000; Yao et al., 2017). Virus was prepared in PBS and used at 5×10^7 PFU per mouse for the recombinant virus or 1×10^8 PFU per mouse for the wild-type virus. Mice were infected intranasally with 25 μL of virus preparation.

Respiratory infection by extracellular bacterial species

A clinical isolate of *Streptococcus pneumoniae* (*S. pneumoniae*) serotype 3 (ATCC 6303; ATCC, Manassas, VA) was prepared and used as previously described (Damjanovic et al., 2013). Briefly, the frozen bacterial stock was plated on blood tryptic soy agar (BD Biosciences, San Jose, CA) supplemented with 5% defibrinated sheep blood (Hemostat, Dixon, CA) and 10 μg/ml neomycin (Sigma-Aldrich, St. Louis, MO) and incubated overnight. Resultant colonies were cultured at 37°C in 5% CO_2 in Todd Hewitt broth (BD Biosciences, San Jose, CA) to mid-logarithmic phase. Bacteria were harvested and resuspended in PBS. The infectious dose was verified by plating 10-fold serial dilutions on blood-agar plates. Mice were infected intratracheally with 5×10^4 (BALB/c mice) or 1×10^4 (C57BL/6 mice) colony-forming units (CFU) of *S. pneumoniae* in 40 μl of PBS. In separate experiments, a clinical isolate *Escherichia coli* (*E. coli*; ATCC 25922; ATCC, Manassas, VA) was prepared by plating and incubating frozen stocks on tryptic soy agar plates and culturing the resultant colonies at 37°C in 5% CO_2 in tryptic soy broth (BD Biosciences, San Jose, CA) to mid-logarithmic phase. The bacteria were harvested and resuspended in PBS. The infectious dose was verified by plating 10-fold serial dilutions on tryptic soy agar plates. Mice were infected intratracheally with 5×10^6 CFUs of *E. coli* in 40 μl of PBS.

Evaluation of clinical outcomes and bacterial infection in tissues

Following bacterial infection, mice were monitored for clinical outcomes including illness scoring (Yao et al., 2017) and body weight changes at various time points, and moribund mice were terminated. The end point was defined as 20% loss of the initial body weight. Otherwise mice were sacrificed at indicated time points post-infection for further analysis including bacterial CFU assay, histopathology, flow cytometry, and chemokine and cytokine analysis. For bacterial CFU assay, the lung and spleen tissues were homogenized in PBS. Serial dilutions of tissue homogenates were plated on blood agar plates (*S. pneumoniae*) or tryptic soy agar plates (*E. coli*), and incubated overnight at 37°C in 5% CO_2. Colonies were counted and calculated as CFU per organ.

Peripheral blood, bronchoalveolar lavage, lung, mediastinal lymph node and bone marrow mononuclear cell isolation

Mice were euthanized by exsanguination. Cells from peripheral blood, bronchoalveolar lavage, lung tissue and mediastinal lymph nodes were isolated as previously described (Jeyanathan et al., 2010, 2017; Yao et al., 2017). Briefly, following exhaustive bronchoalveolar lavage, lungs were cut into small pieces and digested with collagenase type 1 (ThermoFisher Scientific Waltham, MA) at 37°C in an agitating incubator. A single-cell suspension was obtained by crushing the digested tissue through a 100 μm basket filter (BD Biosciences, San Jose, CA). Mediastinal lymph nodes were crushed in PBS by using a pair of frosted glass slides followed by filtering through a 40 μm basket filter (BD Biosciences, San Jose, CA). Heparinized blood was mixed with 10 × volume of ACK lysing buffer (Life Technologies, Grand Island, NY) and incubated at room temperature for 5 min before removing the lysed RBCs upon centrifugation. A second round of RBC lysis was carried out by resuspending the pellet in 2 mL of ACK lysing buffer. Blood leukocytes were then washed in PBS. The spine, femur and tibia bones from donor mice were crushed in a mortar in PBS. Bone marrow cells were filtered through a 40 μm basket filter (BD Biosciences, San Jose, CA) and mixed with 2ml ACK lysis buffer and incubated at room temperature for 2 min. Bone marrow cells were then washed in PBS. Isolated cells were resuspended in either complete RPMI 1640 medium (RPMI 1640 supplemented with 10% FBS and 1% L-glutamine, with or without 1% penicillin/streptomycin) for *ex vivo* culture or in PBS for adoptive transfer or flow cytometry staining.

Immunostaining, *in situ* cell proliferation, and flow cytometry

Cell immunostaining and flow cytometry were performed as previously described (Jeyanathan et al., 2010, 2017; Yao et al., 2017). Briefly, mononuclear cells from bronchoalveolar lavage (BAL), the lung, and peripheral blood were plated in U-bottom 96-well plates at a concentration of 20 million cells/ml in PBS. Following staining with Aqua dead cell staining kit (ThermoFisher Scientific Waltham, MA) at room temperature for 30 min, cells were washed and blocked with anti-CD16/CD32(clone 2.4G2) in 0.5% BSA-PBS for 15 min on ice and then stained with fluorochrome-labeled mAbs for 30 min on ice.

For determination of *in situ* AM proliferation, APC BrdU Flow Kit (BD Biosciences, San Jose, CA) was used. Briefly, intranasal administration of BrdU was performed repeatedly at designated times before or after Ad i.n. at a concentration of 0.5 mg/mouse in a total volume of 50 μL (Jeyanathan et al., 2010). At days 0, 14 or 28, BAL cells were labeled with extracellular mAbs. Stained cells were then fixed and permeabilized with BD Cytofix/Cytoperm followed by incubation in BD Cytoperm Plus buffer. Cells were re-fixed with BD Cytofix/Cytoperm prior to treatment with DNase (30 μg of DNase added to 1×10^6 cells and incubated for 1 h at 37°C). BrdU incorporated into DNA was then detected with an anti-BrdU-APC mAb (clone B44). To determine Ki-67 expression in AM, anti-mouse Ki-67-BV421 mAb (clone 16A8; Biolegend) was used according to manufacturer's instructions. Briefly, BAL cells were labeled with extracellular staining mAbs, followed by resuspension in 70% ethanol and incubation for 1 h at −20°C. Cells were then washed and stained with anti-Ki-67 mAb before flow cytometry analysis.

Fluorochrome-labeled mAbs used for staining pulmonary myeloid cells including AM, interstitial macrophages, monocyte-derived macrophages, monocytes, dendritic cells and neutrophils were anti-CD45-APC-Cy7 (clone 30-F11), anti-CD11b-PE-Cy7 (clone M1/70), anti-CD11c-APC (clone HL3), anti-MHC II-Alexa Flour 700 (clone M5/114.15.2; eBioscience), anti-CD3-V450 (clone 17A2), anti-CD45R-V450 (clone RA3-6B2), anti-Ly6C-Biotin (clone HK1.4; Biolegend), Streptavidin-Qdot800 (Invitrogen), anti-CD24-BV650 (clone M1/69), anti-CD64-PE (clone X54-5/7.1; Biolegend), anti-Ly6G-BV605 (clone 1A8), anti-Siglec-F-PE-CF594 (clone E50-2440), anti-CD80-PerCP-Cy5.5 (clone 16-10A1), anti-CD86-V450 (clone GL1), anti-CD284(TLR4)-APC (clone SA15-21; Biolegend), anti-CD11c-BV711 (clone HL3), anti-CD282(TLR2)-BV421 (clone CB225), anti-CD192(CCR2)-BV421 (clone

SA203G11; Biolegend), anti-Gr-1(Ly6G/Ly6C)-BV605 (clone RB6-8C5), anti-CD45.2-PerCP-Cy5.5 (clone 104), and anti-CD45.1-APC-Cy7 (clone A20). As indicated, some cells were further stained with anti-AnnexinV- APC (eBioscience).

Fluorochrome-labeled mAbs used for T cell surface and intracellular cytokine staining were anti-CD3-V450 (clone 17A2), anti-CD4-PE-Cy7 (clone RM4-5), anti-CD8-APC-Cy7 (clone 53-6.7), anti-IFN-γ-APC (clone XMG1.2). For intracellular cytokine staining in T cells, BAL cells were cultured in the presence of GolgiPlug (5 mg/ml brefeldin A; BD PharMingen) with or without stimulation for 5–6 h with an Ag85A-specific CD8 T cell-specific peptide (MPVGGQSSF) or CD4 T cell-specific peptide (LTSELPGWLQANRHVKPTGS) at a concentration of 1 mg per well. Stimulated cells were stained with cell surface antibodies, followed by fixation/permeabilization by using Fixation/Permeabilization Solution Kit (BD Biosciences, San Jose, CA) according to the manufacturer's instructions. Cells were then stained with anti-IFN-γ-APC mAb in Perm/Wash buffer (BD Biosciences, San Jose, CA) for 30 min on ice.

Unless otherwise indicated, all mAbs and reagents were purchased from BD Biosciences (San Jose, CA). Immunostained cells were processed according to the BD Biosciences instructions for flow cytometry and run on a BD LSR II or BD LSRFortessa flow cytometer. Data were analyzed using FlowJo software (version 10.1; Tree Star, Ashland, OR).

Lung histopathology

At selected time points post bacterial infection, lungs were harvested and inflated with 10% formalin for 72 h. Tissue sections were stained with H&E for histological examination as previously described (Yao et al., 2017). Images of representative micrographs were taken under a Leica DMRA microscope (Leica Microsystems, Wetzlar, Germany) by using Openlab software version 5.0.2 (Improvision, Coventry, UK).

Bone marrow chimeric mice

Bone marrow chimeras were generated as previously described (Bassett et al., 2011). CD45.2 (recipients) and CD45.1 (donors) BALB/c congenic mice were treated with PBS or infected i.n. with virus as above. At four weeks post-viral exposure, recipient mice were irradiated with a single dose of 600 rad γ-ray by using a GammaCell 1000 irradiator (Best Theratronics, Ottawa, ON). At 3 h post-irradiation, single cell suspensions of bone marrow from donor mice were injected i.v. into recipient mice at 5×10^6 BM cells/mouse in 200 μL PBS. Recipient mice were euthanized at 4 and 8 weeks post-bone marrow transplantation for flow cytometry analysis on alveolar macrophages.

Parabiotic mouse model

Parabiotic surgery was conducted as previously described (Ensan et al., 2016). Briefly, the corresponding lateral aspects of two age- and body weight-matched naive mice ($CD45.1^+$ and $CD45.2^+$, respectively) were shaved, and mirroring skin incisions were made in both mice from behind the ear to the tail. The scapulas, and the dorsal and ventral skins were approximated by suture. Three weeks after surgery, both mice were inoculated intranasally with PBS or virus. At 14 and 28 days following inoculation, chimerism in the peripheral blood monocytes, neutrophils and T cells, and airway alveolar macrophages was determined by flow cytometry analysis. Chimerism of each cell population was defined as $\%CD45.1^+ / (\%CD45.1^+ + \%CD45.2^+)$ in $CD45.2^+$ mice, and as $\%CD45.2^+ / (\%CD45.2^+ + \%CD45.1^+)$ in $CD45.1^+$ mice.

Purification of alveolar macrophages, lung $CD11b^+$ or $CD11c^+$ cells, and CD8 T cells

To isolate alveolar macrophages, single cell suspension of BAL was labeled and enriched with CD11c microbeads (Miltenyi Biotec, Auburn, CA) according to the manufacturer's instructions. Purified $CD11c^+$ alveolar macrophages were used for *ex vivo* culture experiments including bacterial stimulation and co-culture with CD8 T cells. Separately, single cell suspension of BAL was labeled with CD11b microbeads (Miltenyi Biotec, Auburn, CA) according to the manufacturer's instructions. The flow-out $CD11b^-$ cells were further labeled with CD11c microbeads. Subsequent $CD11b^-CD11c^+$ alveolar macrophages were used for RNA microarray analysis or *in vivo* adoptive cell transfer experiments. To isolate $CD11b^+$ or $CD11c^+$ lung cells, single cell suspension of the lung was labeled with either CD11b microbeads or CD11c microbeads (Miltenyi Biotec, Auburn, CA) according to the manufacturer's instructions. Purified cells were then used for *ex vivo* culture and *in vivo* adoptive cell transfer. To isolate virus-activated effector CD8 T cells, single cell suspensions from the lung and mediastinal lymph nodes at day 7 post-viral exposure were pooled, followed by CD8 T cell enrichment using a mouse CD8 T cell negative isolation kit (StemCell, Vancouver, BC) according to the manufacturer's instructions. Isolated CD8 T cells were then used for adoptive transfer or *ex vivo* co-culture with alveolar macrophages.

Ex vivo bacterial stimulation, and phagocytosis and killing assays

Isolated alveolar macrophages or lung $CD11b^+/CD11c^+$ cells were resuspended in complete RPMI 1640 medium without penicillin/streptomycin (P/S-free media) and plated at 1×10^6 cells/well in 24-well plates (500 μl/well). Cells were incubated in a 37°C 5% CO_2 cell-culture incubator for 1 h. *S. pneumoniae* was grown as described above. The bacteria were washed twice in PBS and resuspended in P/S free media at 5×10^7 cfu/ml. Bacterial suspension was supplemented with 10% mouse serum (made in house from naive BALB/c mice) and incubate for 30 min at 37°C. Bacteria were supplemented to cell culture wells at a MOI = 10 (5×10^6 cfu of *S. pneumonia* into 5×10^5 cells/well). P/S-free media supplemented with 10% mouse serum was used as control. Cells were then incubated for 1 h at 37°C, followed by supplementing with 1.5 mL complete RPMI 1640 (containing 1% penicillin/streptomycin)/well

and incubation for additional 30 min to kill extracellular bacteria. Bacterial-stimulated cells were then washed twice in PBS and from this point (removal of extracellular bacteria) culture for additional 2 or 12 h before the culture supernatants were collected and stored at −20°C for further chemokine and cytokine assay. Alternatively, bacterial-stimulated alveolar macrophages were lysed at 0, 1, or 2 h post-removal of extracellular bacteria by adding 1 mL per well of autoclaved distilled water. Cell lysates were diluted by 1:5 serial dilutions in PBS, plated on blood agar and cultured overnight. Bacterial phagocytosis and killing were calculated based on the CFUs in the culture plates. In brief, bacterial CFUs at 0 h post bacterial stimulation were calculated as CFU per million alveolar macrophages (phagocytosis). Bacterial CFUs at 1 and 2 h post bacterial stimulation were compared with that at 0 h to show the percentage killing of phagocytosed bacteria.

Isolation of neutrophils from bone marrow and *ex vivo* neutrophil chemotaxis assay

Bone marrow (BM) neutrophils were isolated from naive BALB/c mice via gradient centrifugation of BM single cell suspension. Briefly, BM cells were resuspended in $Ca^{2+}Mg^{2+}$-free HBSS supplemented with 20mM NA-HEPES (pH 7.4) and 0.5% FCS (HBSS-prep) at 1×10^7 cells/ml. Cells (5 mL) were then loaded on 5 mL of 62% Percoll (Sigma-Aldrich, St. Louis, MO) diluted in HBSS-prep in a 15 mL Falcon tube. Cells were centrifuged at 1000 × g for 30 min in a centrifuge at room temperature and with brake off. After gradient centrifugation, neutrophils in the pellet were washed twice in PBS and resuspended in complete RPMI 1640 for *ex vivo* chemotaxis analysis.

Ex vivo neutrophil chemotaxis analysis was performed in a 96-well ChemoTx microplate with 3 μm pore size (Neuro Probe, Gaithersburg, MD). Briefly, 29 μL of PBS, diluted lung homogenates in PBS, BAL fluids with anti-mouse MIP-2 rabbit anti-serum or control rabbit serum, culture supernatants of bacterial-stimulated alveolar macrophages with anti-mouse MIP-2 rabbit anti-serum or control rabbit serum, were plated in the bottom wells. Neutrophils (5×10^6 cells/ml) in 20 μL were added to the plater filter/insert and placed to the top of sample wells. The plate was incubated for 2 h in a 37°C 5% CO_2 cell culture incubator. Inserts were then removed and cells in the bottom wells were diluted 1:1 in Turk Blood Dilution Fluid (RICCA Chemical, Arlington, TX) and counted under microscope. Neutrophil chemotaxis was expressed as percentage of the cell counts in bottom wells divided by the starting cell number (1×10^5 cells).

In vivo depletion of T cells, neutrophils, and monocytes

To deplete CD4 T and/or CD8 T cells *in vivo*, mice were injected i.p. with 200 μg of anti-CD4 mAb (clone GK1.5) and/or 200 μg of anti-CD8 mAb (clone 2.43). To achieve continuous T cell depletion, repeated doses of 100 μg of anti-CD4 mAb and/or 100 μg of anti-CD8 mAb were administered i.p. at a 7-day interval as needed. To partially or completely deplete neutrophils *in vivo*, mice were injected i.p. with 100 μg or 200 μg of anti-Ly6G mAb (clone 1A8 purchased from UCSF Monoclonal Antibody Core, San Francisco, CA) or 200 μg of isotype control mAb (clone 2A3; BioXCell, West Lebanon, NH) at 1 h post-bacterial challenge. To deplete blood monocytes *in vivo*, viral-exposed $CCR2^{-/-}$ mice were injected intravenously with Clodronate liposomes or control liposomes (both from FormuMax Scientific, Sunnyvale, CA) at 200 μl/mouse/day for 4 consecutive days following virus inoculation (Ensan et al., 2016).

In vivo reconstitution of IFN-γ

In selected experiments, repeated doses of recombinant murine IFN-γ protein (rIFN-γ, PeproTech, Rocky Hill, NJ) were administered i.n. to IFN-$\gamma^{-/-}$ mice at 1.2 μg /mouse/dose on days 4, 6, 8 and10 post-viral exposure. At day 28 post-viral exposure, BAL cells were obtained for flow cytometry analysis and *ex vivo* bacterial stimulation.

In vivo and *ex vivo* MIP-2 neutralization

For neutrophil chemokine MIP-2 neutralization, 200 μg of rabbit anti-murine MIP-2 polyclonal Abs in serum (kindly provided by Dr. C. Hogaboam)(Damjanovic et al., 2013) or normal rabbit serum as control was injected i.p. into mice immediately after bacterial infection. Mice were sacrificed at either 24 h to determine pulmonary neutrophilia or 72 h post-infection to determine bacterial counts in the tissue. For *ex vivo* MIP-2 neutralization, rabbit anti-murine MIP-2 serum or normal rabbit serum was added to samples at 1:4 volume, followed by neutrophil chemotaxis analysis.

Ex vivo co-culture of alveolar macrophages and CD8 T cells

Viral-exposed mice were depleted of T cells by *in vivo* administration of anti-CD4 and anti-CD8 mAbs from day 3 post-virus inoculation. On day 7 post-viral exposure, AM were isolated from the BAL of T cell-depleted mice. CD8 T cells were purified from the lung and mediastinal lymph nodes from the mice without T cell depletion. AM were co-cultured with CD8 T cells at 1:5 ratio in 24-well plates (100,000 alveolar macrophages per well) in 1 mL complete RPMI 1640 for 24 h in a 37°C 5% CO_2 cell-culture incubator. In selected wells, CD8 T cells were separated with AM by using a transwell insert with 0.4 μm pore size (Corning, Tewksbury, MA). AM from mice at day 7 post-viral exposure without T cell depletion were used as control. Cells were recovered for flow cytometry analysis on alveolar macrophages.

Chemokine and cytokine quantification

Chemokines including MIP-2, KC, IP-10, MCP-1 and MIP-1α were quantified by using MCYTOMAG-70K mouse chemokine and cytokine detection kit (Millipore Sigma, Etobicoke, ON) according to the manufacturer's instructions. Plates were read on a MagPix

reader (ThermoFisher Scientific Waltham, MA) by using a xPONENT software (ThermoFisher Scientific Waltham, MA). Concentrations of chemokines were calculated based on serial dilutions of standards by using spline curve fitting in GraphPad Prism software (Version 6, GraphPad Software, La Jolla, CA). Proinflammatory or immune cytokines IFN-γ and IL-1β were quantified by using DuoSet ELISA kit (R&D Systems, Minneapolis, MN) according to the manufacturer's instructions. ELISA plates were read on a spectrophotometer at 450 nm.

RNA isolation and gene microarray

Alveolar macrophages from 4-week PBS or viral-exposed mice were purified from the BAL as described above. Cells from each 3 mice were pooled and used as one sample and triplicate samples/group were set up for RNA extraction and gene microarray analysis as previously described (Jeyanathan et al., 2017). Briefly, total cellular RNA was isolated using an RNeasy mini kit (QIAGEN, Germantown, MD). Disrupted cells in RLT buffer were processed according to the manufacturer's instructions. RNA was eluted using 14 μL of RNase-free water. RNA samples were stored at -80°C until use. Quality of RNA and subsequent microarray was carried out by the Center for Applied Genomics of The Hospital for Sick Children (Toronto, ON). The quality of RNA samples was analyzed using the Agilent 2100 bioanalyzer, which uses RNA 6000 Nano LabChip platform (Agilent Technologies Canada, Mississauga, ON). RNA samples were then subjected to RNA microarray expression analysis using the Affymetrix Mouse Gene 2.0 ST array. This array contains protein-coding regions.

Microarray analysis

Genome-wide gene expression analysis was performed using Affymetrix Mouse Gene 2.0ST microarrays (Microarray facility, Center for Applied Genomics of The Hospital for Sick Children, Toronto, Ontario, Canada). Groups were compared and genes found to be differentially expressed with a corrected p value of < 0.05 and an absolute fold change of at least 1.5 were used to find regulation of Gene Ontology Biological Processes terms (Jeyanathan et al., 2017). Differential expression of genes belonging to "Defense response to bacterium (GO ID:42742)," "Chemotaxis (GO ID: 6935)," and "Antigen processing and presentation (GO ID:19882)" terms were visualized in heatmaps.

Metabolic assay of alveolar macrophages

Real-time cell metabolism of alveolar macrophages was determined by using the Seahorse XF Glycolysis Stress Test Kit (Agilent Technologies, Santa Clara, CA) according to the manufacturer's instructions. Alveolar macrophages were obtained from the BAL, following T cell negative selection by using CD3ε microbeads (Miltenyi Biotec, Auburn, CA). Purified alveolar macrophages were seeded onto a 24-well microplate (Agilent Technologies, Santa Clara, CA) at a density of 2×10^5/well. The plate was incubated for 2 h in a 37°C 5% CO_2 cell culture incubator and washed twice with culture media to further remove non-adhering cells. Alveolar macrophages were then incubated overnight in complete RPMI 1640 supplemented with 10mM HEPES, 0.5mM Na pyruvate, 55 μM 2-Mercaptoethanol, 0.1mM NEAA in a 37°C 5% CO_2 cell culture incubator. On the following day, alveolar macrophages were washed twice and cultured with Seahorse XF base medium supplemented with 2 mM L-glutamine (Agilent Technologies, Santa Clara, CA) for the duration of the assay. Extracellular Acidification Rates (ECAR) was assessed by using a Seahorse XFe24 Analyzer (Agilent Technologies, Santa Clara, CA). Glycolysis was represented by ECAR after the addition of 10 mM glucose. Glycolytic capacity was represented by maximum ECAR following the addition of 1 μM oligomycin. Glycolytic reserve was represented by the difference between glycolytic capacity and glycolysis. Data were analyzed using Wave Desktop software version 2.6 (Agilent Technologies, Santa Clara, CA) and normalized to protein.

QUANTIFICATION AND STATISTICAL ANALYSIS

Statistical parameters including the exact value of n, the definition of center, dispersion and precision measures, and statistical significance are reported in Figures and Figure Legends. A p value of < 0.05 was considered significant (*$p < 0.05$, **$p < 0.01$, ***$p < 0.001$, ****$p < 0.0001$). A two-tailed Student t test was performed for pairwise comparisons. One-way ANOVA followed by a Tukey test was performed to compare more than two groups. All analyses were performed by using GraphPad Prism software (Version 6, GraphPad Software, La Jolla, CA). For microarray data analysis, all statistical analyses were performed in R version 3.3.0 and various Bioconductor packages (Jeyanathan et al., 2017). Principal Component Analysis (PCA) was performed using *rgl* package (https://cran.r-project.org/web/packages/rgl/index.html); hierarchical clustering and heatmaps were obtained using *gplots* package (https://cran.r-project.org/web/packages/gplots/index.html); differential expression analysis was performed using *limma* package with p values corrected by using the Benjamini-Hochberg procedure. Gene Ontology analysis was performed using BINGO plugin in Cytoscape environment (Jeyanathan et al., 2017).

DATA AND SOFTWARE AVAILABILITY

Raw data files for the RNA microarray analysis have been deposited in the NCBI Gene Expression Omnibus under accession number GEO: GSE118512.

Cell

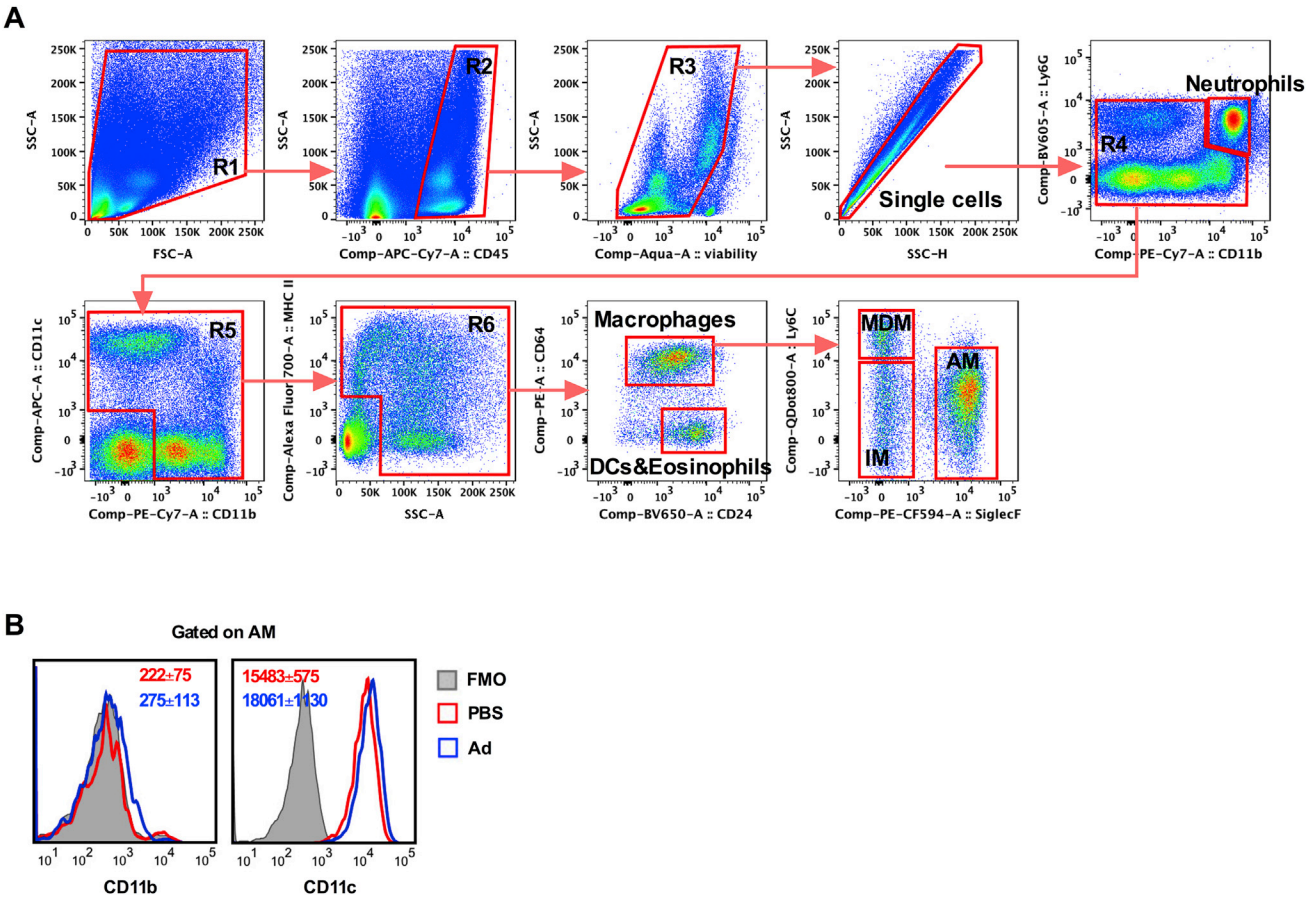

Figure S1. Flow Cytometric Gating Strategy Used to Separate Alveolar Macrophages from Other Major Myeloid Cell Populations, Related to Figures 1, 2, 3, and 4

(A) Gating strategy (R–gated region) applied in this study to precisely distinguish alveolar macrophages (AM) from other major myeloid cell populations including dendritic cells (DCs), interstitial macrophages (IM) and monocyte-derived macrophages (MDM) in the airway lumen (BAL) or lung tissue, based on a comprehensive flow cytometry immunostaining panel. The example shown here was on lung tissue-derived mononuclear cells isolated from day 28-infected animals, in order to better display the overall gating strategy and various myeloid cell populations. The BAL samples had few neutrophils, MDM and IM.

(B) Surface expression of CD11b and CD11c in AM in PBS- or viral-exposed mice at 28 days post-infection.

Numbers in (B) represent mean ± SD of median fluorescence intensity (MFI). Data are representative of three independent experiments with n = 3 mice/group.

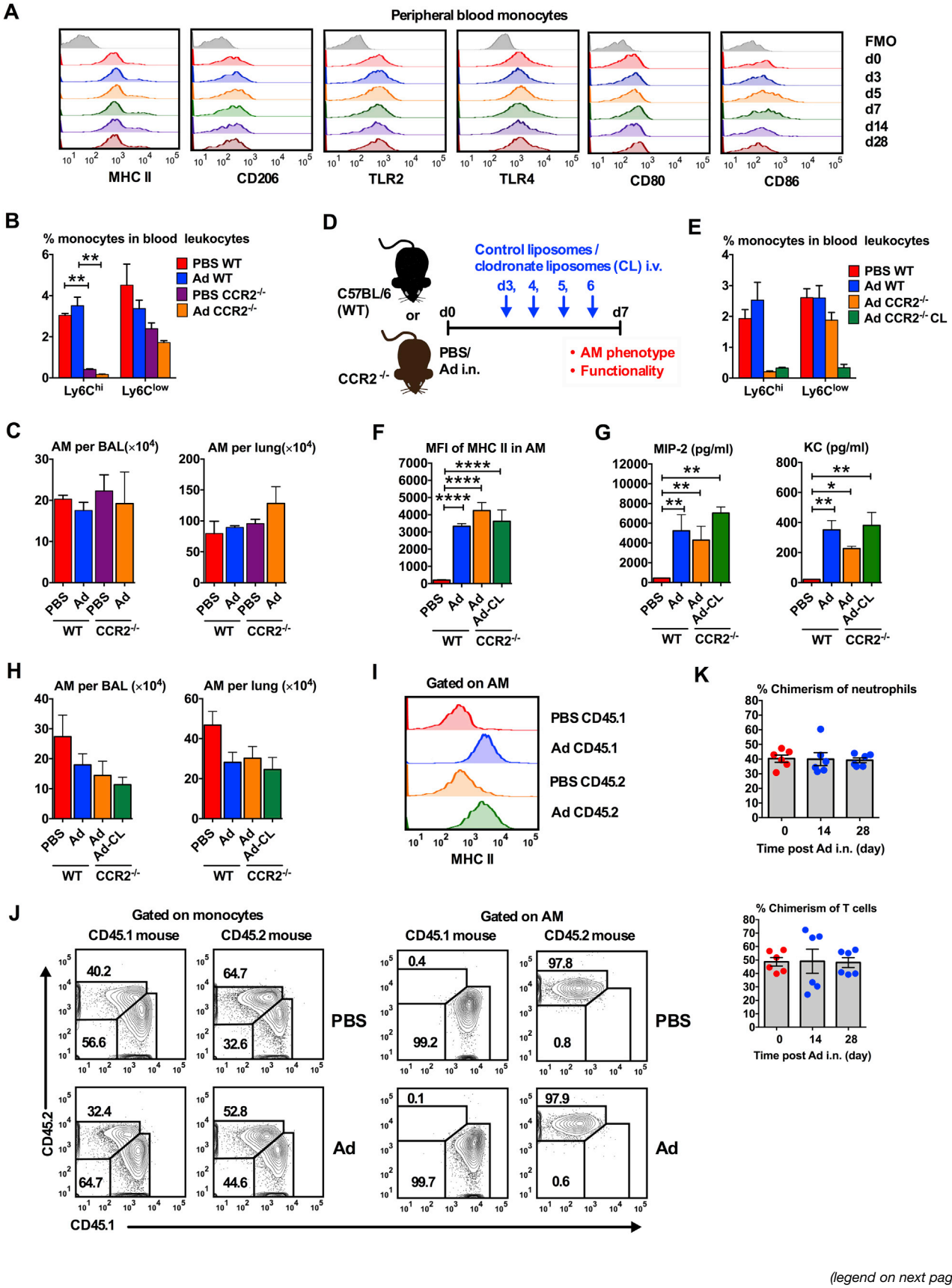

(legend on next page)

Figure S2. Characterization of Peripheral Blood Monocytes and Alveolar Macrophages in Viral-Exposed Monocyte-Deficient or Parabiotic Mice, Related to Figure 2

(A) Histograms of expression of MHC II and activation-associated surface molecules on circulating blood monocytes at various time points post-viral infection.
(B) Frequencies of Ly6C^{hi} and Ly6^{low} monocytes in peripheral blood leukocytes in 4-week PBS control or viral-exposed wild-type (WT) and CCR2-deficient (CCR2$^{-/-}$) mice.
(C) Numbers of total AM in BAL and lung of 4-week PBS control or viral-exposed WT and CCR2$^{-/-}$ mice.
(D) Schematic representation of clodronate liposomes (CL)-mediated monocyte depletion in viral-infected WT C57BL/6 or CCR2$^{-/-}$ mice.
(E) Frequencies of Ly6C^{hi} and Ly6^{low} monocytes in peripheral blood leukocytes in 7-day PBS control or viral-exposed WT and CCR2$^{-/-}$ mice injected repeatedly with control or clordonate liposomes (CL).
(F) Representative histograms and MFI of MHC II expression on AM of 7-day PBS control or viral-exposed WT and CCR2$^{-/-}$ mice injected with control or clordonate liposomes (CL).
(G) Concentrations of MIP-2 and KC in culture supernatants of *ex vivo S. pneumoniae*-stimulated AM from 7-day PBS control or viral-exposed WT and CCR2$^{-/-}$ mice injected with control or clordonate liposomes (CL).
(H) Numbers of total alveolar macrophages (AM) in the BAL and lung of 7-day PBS control or viral-exposed WT and CCR2$^{-/-}$ mice injected with control or clordonate liposomes (CL).
(I) Representative histograms of expression of MHC II in airway AM of PBS control or viral-exposed parabiotic congenic mice.
(J) Representative flow cytometry dotplots of CD45.1^{+} and CD45.2^{+} circulating monocytes and AM of PBS control or viral-exposed parabiotic mice. Numbers represent percentage of cells in each gate against the parental gate.
(K) Chimerism of neutrophils and T cells in blood of PBS control or viral-exposed parabiotic mice.
Bar graphs in B-H are presented as mean ± SD. Bar graphs in K are presented as mean ± SEM. Data are representative of two independent experiments with n = 3 mice/group in A-C and n = 6 mice/group in I-K. Data in E-H are from one experiment with n = 3 animals/group. *$p < 0.05$; **$p < 0.01$; ****$p < 0.0001$.

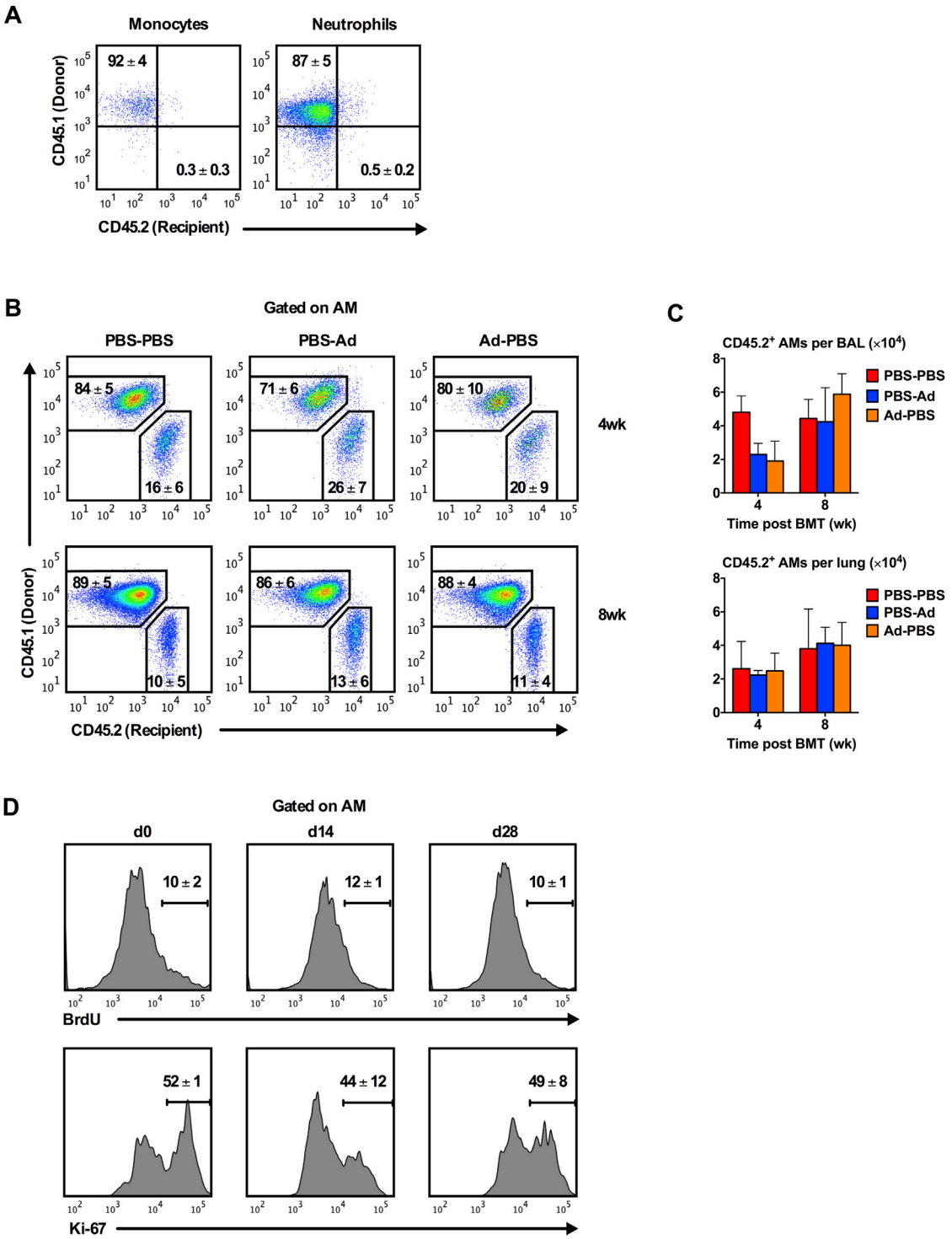

Figure S3. Frequencies and/or Numbers of Donor- and Recipient-Derived Peripheral Blood Monocytes and Neutrophils and Total Alveolar Macrophages in the Lung of Congenic Bone Marrow Chimeric Mice, Related to Figure 2

(A) Representative flow cytometry dotplots of donor (CD45.1$^+$)- and recipient (CD45.2$^+$)-derived peripheral blood monocytes and neutrophils at 4 weeks post-3-way bone marrow transplantation (BMT).

(B) Representative dotplots of donor- and recipient-derived alveolar macrophages (AM) in the BAL at 4 and 8 weeks post-BMT.

(legend continued on next page)

(C) Numbers of radio-resistant, self-sustainable recipient ($CD45.2^+$)-derived total AM in the BAL and lung in BM chimeric mice at 4 and 8 weeks post-BMT. (D) Representative histograms of airway AM incorporated with BrdU or stained positive for Ki-67 protein at day 0, and day 14 and 28 post-viral infection. Numbers in A/B/D represent mean ± SD of percentage cells in each gate against parental gate. Bar graphs in C are presented as mean ± SD. Data are from one experiment with n = 5 mice/group.

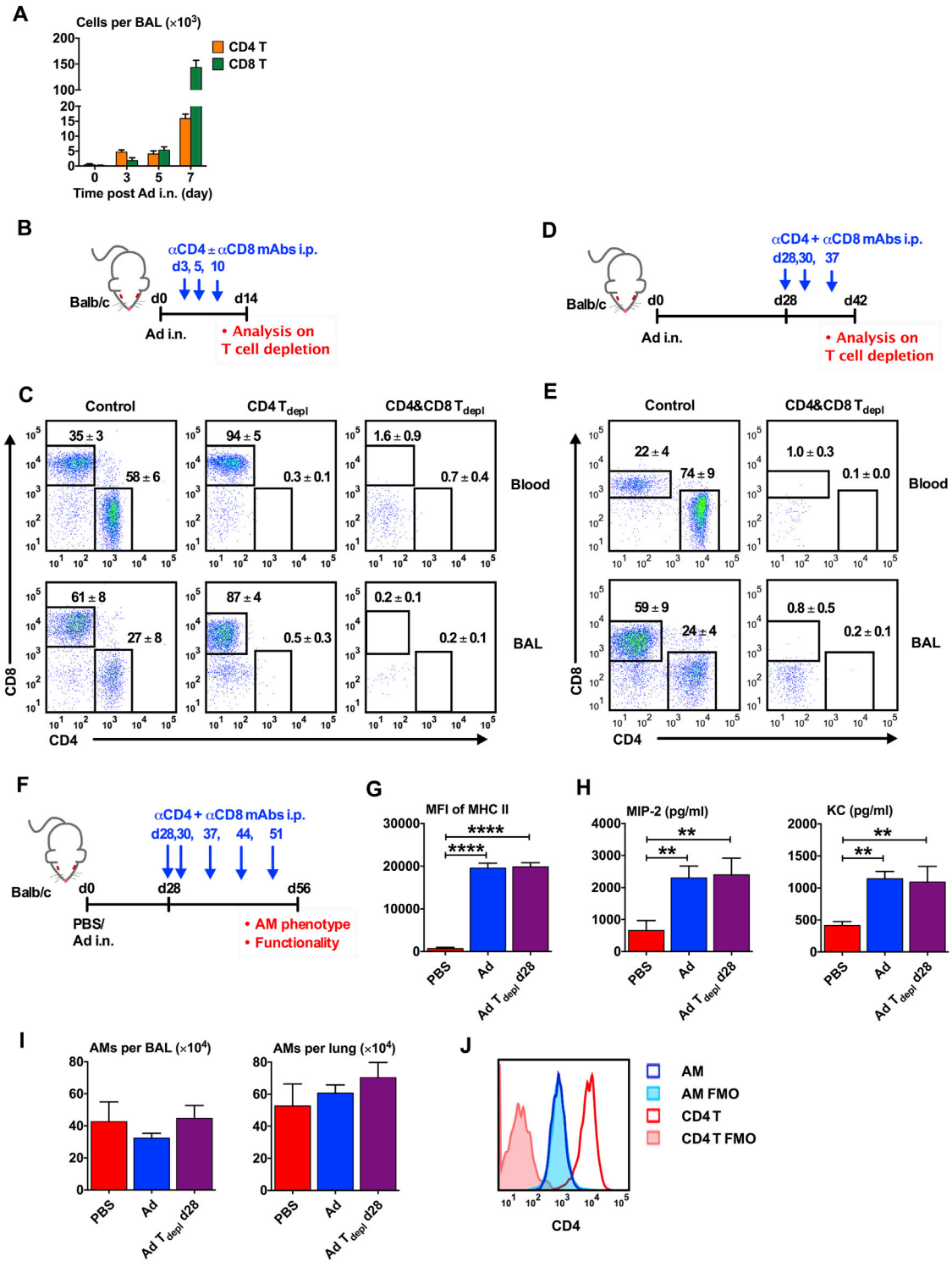

Figure S4. Early Effector T Cell Responses Post-Viral Exposure, Efficiency of T Cell Depletion, and Lack of Effects on Memory Alveolar Macrophage Generation when T Cells Were Depleted from Day 28 onward, Related to Figure 3

(A) Numbers of total CD4 T and CD8 T cells in the airway (BAL) during the effector phase (days 0, 3, 5 and 7) of host immune responses to viral infection.

(B) Schema of T cell depletion from day 3 post-viral infection.

(C) Representative flow cytometry dotplots of T cells in blood and airway with or without T cell depletion beginning from day 3 post-viral infection.

(D) Schema of T cell depletion beginning from day 28 post-viral infection.

(legend continued on next page)

(E) Representative flow cytometry dotplots of T cells in blood and airway with or without T cell depletion from day 28 post-viral infection.
(F) Schematic experimental design to examine the role of T cells in maintenance of fully developed memory AM following viral infection.
(G) MFI of MHC II expression on airway AM harvested at 56 days post-infection with or without T cell depletion carried out during the maintenance phase of memory AM.
(H) Concentrations of MIP-2 and KC in culture supernatants of *ex vivo S. pneumoniae*-stimulated AM from day-56 PBS or viral-exposed mice with or without T cell depletion carried out during the maintenance phase of memory AM.
(I) Numbers of AM in the BAL and lung from day-56 PBS or viral-exposed mice with or without T cell depletion carried out during the maintenance phase of memory AM.
(J) Representative histograms of CD4 expression on airway AM and CD4 T cells.
Bar graphs are presented as mean ± SD. Numbers in C and E represent mean ± SD of percentage cells in each gate against parental gate. Data are representative of two independent experiments with n = 3 mice/group. $^{**}p < 0.01$; $^{****}p < 0.0001$.

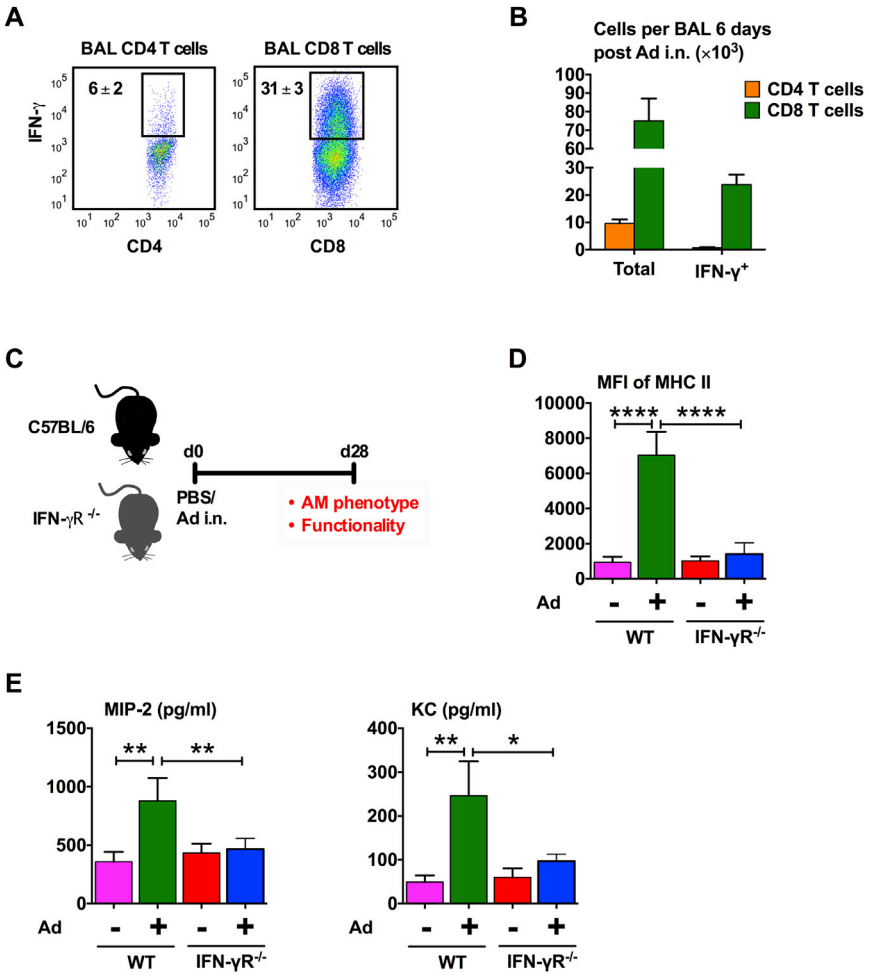

Figure S5. IFN-γ Production by CD8 and CD4 T Cells in the Airway during the Effector Phase of Host Immune Responses to Viral Infection and Requirement of IFN-γ Receptor for AM Memory Generation, Related to Figure 4

(A) Frequencies of IFN-γ+ CD8 and CD4 T cells in the airway (BAL collected at day 6 post-viral infection in BALB/c mice. The analysis was carried out by intracellular cytokine staining on Ag-stimulated T cells.

(B) Numbers of total CD4 and CD8 T cells or numbers of IFN-γ+ CD8 and CD4 T cells in the BAL collected at day 6 post-viral infection in BALB/c mice.

(C) Schematic experimental design of WT C57BL/6 and IFN-γ receptor deficient (IFN-$\gamma R^{-/-}$) mouse model of respiratory viral infection.

(D) MFI of MHC II expression on airway AM at 28 days post-viral infection in WT and IFN-$\gamma R^{-/-}$ mice.

(E) Concentrations of MIP-2 and KC in culture supernatants of *ex vivo S. pneumoniae*-stimulated AM from 28-day infected WT or IFN-$\gamma R^{-/-}$ mice.

Bar graphs are presented as mean ± SD. Data are representative of two independent experiment with n = 3 mice/group. *p < 0.05; **p < 0.01; ****p < 0.0001.

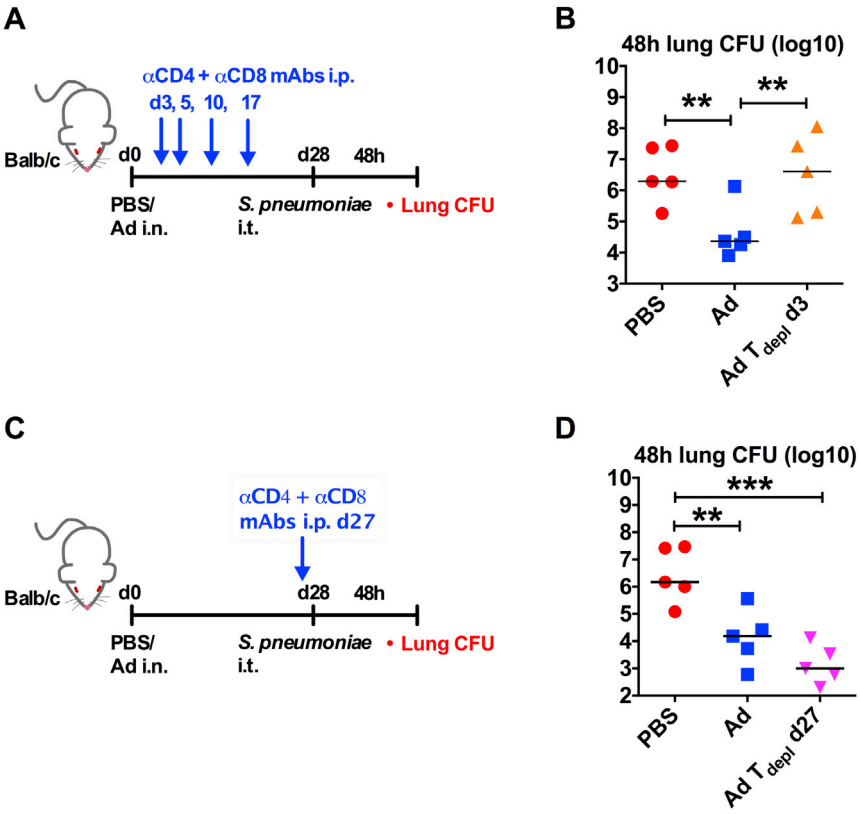

Figure S6. Differential Involvement of Virus-Induced T Cells in Trained Innate Immunity against Bacterial Infection, Related to Figure 5

(A) Schematic experimental design of studying the effect of CD4 and CD8 T cell depletion on anti-bacterial trained innate immunity by repeated injections of T cell-depleting mAbs during the effector phase of host immune responses to respiratory viral exposure in BALB/c mice.

(B) Bacterial counts (CFU) in the lung at 48 h post-bacterial infection in mice of PBS control or viral-exposure with or without T cell depletion carried out during the effector phase.

(C) Schematic representation of experimental design of studying the effect of CD4 and CD8 T cell depletion on anti-bacterial trained innate immunity by injection of T cell-depleting mAbs during the memory phase of host immune responses to respiratory viral exposure in BALB/c mice.

(D) Bacterial counts (CFU) in the lung at 48 h post-bacterial infection in mice of PBS control or viral-exposure with or without T cell depletion carried out during the memory phase. Horizontal lines in scatter dotplots represent median values. Data are representative of two independent experiments with n = 5 mice/group. $^{**}p < 0.01$; $^{***}p < 0.001$.

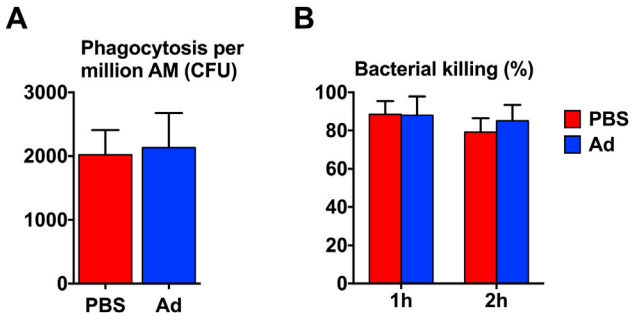

Figure S7. Comparison of Bacterial Phagocytosis and Killing Capacities of Conventional and Memory Alveolar Macrophages, Related to Figure 6

(A) Phagocytosis as intracellular CFU of *S. pneumoniae* by alveolar macrophages (AM) isolated from 4-week PBS control and viral-exposed BALB/c mice.
(B) Killing rates of phagocytosed *S. pneumoniae* by AM isolated from 4-week PBS control and viral-exposed BALB/c mice at 1 and 2 h post-*ex vivo* bacterial infection. Bar graphs are presented as mean ± SD. Data are representative of two independent experiments with triplicate wells/group.